UNIVERSIDAD
NACIONAL
DE COLOMBIA

Dinámica de fluidos computacional como herramienta para el diseño de micromodelos para la evaluación de inyección de surfactantes en procesos de recobro mejorado

Santiago Céspedes Zuluaga

Universidad Nacional de Colombia
Facultad de minas, Departamento de procesos y energía
Medellín, Colombia
2020

Computational Fluid Dynamics as a Tool for the Design of Micromodels for the Evaluation of Surfactant Injection in Enhanced Oil Recovery Processes

Santiago Céspedes Zuluaga

Tesis o trabajo de investigación presentada(o) como requisito parcial para optar al título de:

(A dissertation presented in partial fulfilment of the requirements for the degree of):

Magister en Ingeniería Química

Master in Chemical Engineering

Director (Supervisor):

Ph.D., Alejandro Molina Ochoa

Codirector (Co-supervisor):

Ph.D., Farid B. Cortés Correa

Línea de Investigación (Research field):

Enhanced Oil Recovery

Grupo de Investigación (Research group):

Fenómenos de superficie – Michael Polanyi

Universidad Nacional de Colombia

Facultad de minas, Departamento de procesos y energía

Medellín, Colombia

2020

A mis padres que siempre me apoyan y para Anderson que nunca será olvidado.

Acknowledges

Professor Alejandro Molina, Full Professor. Departamento de Procesos y Energía. Universidad Nacional de Colombia – Sede Medellín (Medellín-Colombia).

Professor Farid Cortés, Full Professor. Departamento de Procesos y Energía. Universidad Nacional de Colombia – Sede Medellín (Medellín-Colombia).

Grupo de investigación en Fenómenos de Superficie - Michael Polanyi. Facultad de minas. Universidad Nacional de Colombia – Sede Medellín (Medellín-Colombia).

The author acknowledges COLCIENCIAS, ANH, and Universidad Nacional de Colombia for their financing and logistic support provided by agreement 064-2018.

Abstract

Computational fluid dynamics (CFD) was used to propose a guide for the design of a microfluid device that would make more evident differences in the performance of surfactants with similar properties in the ultra-low range of interfacial tension during Chemical Enhanced Oil Recovery (CEOR). In surfactant injection, one of the most widely applied CEOR methods, the objective is to decrease the interfacial tension of the phases present in the reservoir. The CFD simulations were carried out using the Volume of Fluid (VOF) method for a fully meshed porous geometry generated using a triangular mesh from the Meshing software present in the Ansys simulation package. The CFD analysis considered the effect of the interfacial tension of two surfactants (0.037 mN/m and 0.045 mN/m) on the oil recovery factor, the breakthrough time, the fractal dimension of the flow pattern, the pressure drop, and the entrapment effect. The properties of the microfluid system that were addressed in the simulation were porosity (50%-70%), grain shape (circular and irregular), presence or absence of fractures, and injection velocity (10 ft/day - 30 ft/day). The methodology described in the guide indicates that for the pair of surfactants selected, a microfluid device with a porosity of 0.5, circular grains, the presence of a fracture and operating at the maximum injection velocity (30 ft/day) could better identify differences in the performance of both surfactants. The guide developed in this research will facilitate the design of micromodels by coupling this technology with CFD simulation techniques.

Keywords: Computational fluid dynamics simulations; CEOR; microfluidics.

Resumen

Se usó la dinámica de fluidos computacional (CFD) con el fin de proponer una guía para el diseño de dispositivos de microfluídica donde la diferencia entre dos surfactantes con propiedades similares en el rango ultra bajo de tensión interfacial se haga mas evidente durante procesos de recuperación química mejorada de petróleo (CEOR). En la inyección de surfactantes, uno de los métodos CEOR más ampliamente aplicados, el objetivo es disminuir la tensión interfacial de las fases presentes en el yacimiento. Las simulaciones de CFD se llevaron a cabo utilizando el método multifásico Volume of Fluid (VOF) para una geometría de un medio poroso con un mallado triangular generado a partir del software Meshing presente en el paquete de simulación de Ansys. El análisis CFD consideró el efecto de la tensión interfacial de dos surfactantes (0.037 mN /m y 0.045 mN/ m) sobre el factor de recobro, el tiempo de ruptura, la dimensión fractal del patrón de flujo, la caída de presión y el efecto de entrampamiento. Las propiedades de los dispositivos de microfluídica que se abordaron en la simulación fueron porosidad (50% -70%), forma de grano (circular e irregular), presencia o ausencia de fracturas y velocidad de inyección (10 ft/day - 30 ft/day). La metodología descrita en la guía indica que, para el par de surfactantes seleccionados, un micromodelo con una porosidad de 0.5, granos circulares, la presencia de una fractura y el funcionamiento a la velocidad máxima de inyección (30 pies / día) podría identificar mejor las diferencias en el rendimiento de ambos surfactantes. La guía desarrollada en esta investigación facilitará el diseño de micromodelos al acoplar esta tecnología con técnicas de simulación de CFD.

Palabras clave: Dinámica de Fluidos Computacional; CEOR; microfluídica.

Content

List of figures

Pág.

Chapter 1

Chapter 2

List of tables

Pág.

Chapter 2

List of symbols and abbreviations

Symbol	
α_i	Volume fraction of phase i
ρ	Density
μ	Viscosity
$\vec{u}$	Velocity vector
p	Pressure
$\vec{F}$	Surface tensión force
κ	Curvature of interface

Abbreviations	
CEOR	Chemical Enhanced Oil Recovery
CFD	Computational Fluid Dynamics
CSF	Continuum Surface Force
EOR	Enhanced Oil Recovery

Introduction

Due to population growth and resource consumption, in recent years world energy demand has increased. Also, it is expected that by 2030, crude oil will be approximately 30% of the primary energy available [1]. Because of this projection, it is necessary to develop technologies that allow oil extraction more efficiently.

At present, there are three techniques for oil recovery: primary recovery, secondary recovery, and tertiary recovery, the latter, also known as enhanced oil recovery (EOR). From the primary and secondary recovery, approximately 35% of the oil available in the reservoir is extracted, leaving most of this fluid trapped in the porous medium [2]. EOR processes, which groups different techniques focused on increasing the recovery factor, modify the properties of the fluids and materials present in the reservoir to facilitate the oil movement.

One of the EOR techniques is the injection of chemicals, in which the surfactant injection is one of the leading and most studied processes for the reduction of interfacial tension, where capillary forces seek the trapped oil release within the reservoir [3].

The evaluation of EOR technologies, particularly surfactant injection, is carried out experimentally in synthetic cores, where it is necessary to use different devices that control flows and pressures. Furthermore, visualization of the processes that occur within these devices is not allowed (black box devices). [4].

Microfluidic devices have been an excellent option to overcome the problems presented in core injection tests [5-7]. Micromodels can handle small volumes of fluids where liquid handling is secure, and process times are shorter than core injection tests [8, 9]. Also, microfluidic devices help to visualize the flow patterns during oil displacement tests, which facilitates the phenomena characterization in injection processes [10-12]. Due to

micromodels advantages, in recent years, there has been a growing interest in the design, characterization, and use of these devices [13-16].

Owing to the large number of factors that affect the chemical enhanced oil recovery (CEOR) processes, specifically surfactants injection, it is necessary to evaluate different characteristics in order to optimize the process. At this point, the use of technologies such as micromodel devices allows testing with a lower resource expenditure, where the tests are carried out in a controlled environment. The favorable characteristics presented by the micromodels allow the evaluation of multiple factors in the oil recovery processes. However, due to the complexity of each reservoir, the micromodels must be adjusted to a need. In this way, the design of these devices, specifically the geometry of the medium, plays an important role.

For the design of microfluidic devices, it is necessary to know the characteristics of the porous medium and the properties of the fluids that interact within these [17, 18]. Additionally, if it is desired to study a particular phenomenon or characteristic of the CEOR process, it is necessary to consider properties in the micromodels such as morphology, pore pattern (perfectly regular, partially regular, fractal patterns, and irregular patterns [9]), fluid injection point, material characteristics, among others, that allow the desired process development [19, 20]. This work can be carried out through multiple experimental tests or numerical modeling of the multiphase flow within these devices [14, 15, 17, 21]. Another alternative for the design of these devices is a real replica of the porous medium where the EOR process is performed; this is done through scanning electron microscope (SEM) images of the specific medium to be studied, where the images are used to process in a computer and finally, through the engraving technique, this geometry is captured in a material [18, 22]. The latter technique has the advantage of being able to constitute the porous medium more accurately, but it is a unique representation of the medium studied where the use of this geometry is limited by the conditions of the sample taken for the SEM image, in addition, the use of these processes represents high investments due to the costs associated with obtaining a representative sample of an oil deposit.

Micromodels can be experimentally designed to identify differences in the performance of surfactants during EOR [23-25]. A disadvantage of a solely-experimental approach for the design of microfluid devices is the heuristic characteristic of the method where time and raw

material are invested in different models that may not serve practical purposes. Numerical modeling presents an alternative to the experimental approach, particularly if it follows a methodology that allows the design of micromodels for the evaluation of different characteristics in EOR processes with surfactant injection.

Computational fluid dynamics (CFD) is a technique used to study systems that involve fluid flow, heat transfer, among other phenomena through computer-solved algorithms [26]. CFD has some advantages over experimental tests where the short evaluation time, the savings in the material used, and the ability to evaluate critical and special situations that can hardly be obtained in a laboratory stand out [21, 27].

In this way, CFD is presented as a tool for the evaluation of CEOR processes by simulating micromodels, with the advantage of manipulating fluid conditions or the environment where the process is carried out. CFD simulations enable the evaluation of differences on the performance of surfactants in short times and with low cost.

In this research, CFD was used to simulate the injection of surfactants to modified micromodels. Once the CFD simulations were validated with experimental data available in the literature [28], the effect of several characteristics of the microfluidic setup (porosity, grain shape, presence of fractures, and injection velocity) on typical metrics (the recovery factor, breakthrough time, fractal dimension, pressure drop, and entrapment effect) of the surfactant performance was studied.

The main objective of this research was to propose a methodology for the design of micromodels for the evaluation of surfactant injection in enhanced oil recovery processes through the analysis in computational fluid dynamics. To achieve the main objective, the following specific objectives were proposed:

- Characterize the micromodels that are currently on the market for the evaluation of surfactant injection by CFD.
- Propose different configurations of micromodels that represent the characteristic phenomena involved in the surfactant injection processes through CFD analysis.
- Determine a micromodel selection route to evaluate surfactant injection processes for enhanced oil recovery processes.

This document has three chapters. Chapter 1 deals with the fundamentals concepts for research development and offers a review of concepts related to microfluidics along with the mathematical modeling of the CEOR process through CFD simulations. Particularly, sections 1.5 to 1.6 present the characterization of micromodels used for the evaluation of surfactant injection. Chapter 2 is written as a freestanding manuscript and follows the format of a journal paper. It is in this Chapter 2 where different configurations of micromodels are proposed and where the micromodel selection route is defined. Finally, Chapter 3 contains the conclusions and recommendations for future work.

1. Fundamentals of microfluidic devices processes and CFD simulation

This chapter describes theoretical concepts that are important for the development of this thesis. It also presents methods used in the characterization of the processes carried out in microfluidic devices and describes the mathematical model used to perform the CFD simulations along with a review of previous research in this area.

1.1 Enhanced Oil Recovery Methods

In the crude oil extraction process, there are three stages identified as primary, secondary, and tertiary recovery. In primary recovery, the energy contained in the oilfield is used to mobilize and extract oil. When the reservoir does not contain enough energy to continue the oil production process, it is necessary to inject fluids that are natural to the reservoir (water, gas) to maintain a pressure that allows normal production, this process is known as secondary recovery [29]. Finally, after the processes described, approximately 65% of the original crude oil in the reservoir is trapped inside due to capillary forces. EOR processes are used to take advantage of this extraction potential. EOR techniques consist of the injection of chemicals or substances that modify the properties of the reservoir and fluids to increase oil production [2].

EOR processes are grouped into three categories: (i) chemical and (ii) thermal methods, and miscible displacement [30]. Chemical methods involve the injection of different substances into the reservoir to change the interactions between the fluids and the porous medium to improve the displacement of the crude oil. In thermal methods, heat is injected into the reservoir to decrease the crude oil viscosity and, therefore, to increase oil mobility, which leads to easy oil extraction. Finally, miscible displacement consists of the injection of gases that reduces the interfacial tension between the crude oil and the displacing fluid and facilitates the mobilization of the crude oil.

1.2 Chemical Enhanced Oil Recovery Methods

As previously mentioned, this recovery method involves the injection of chemical agents into the reservoir to modify properties in it and thus facilitate oil extraction. Usually, the substances involved in this process are surfactants, polymers, and alkaline substances [2, 3, 30, 31]. The objective of the injection of surfactant and alkaline substances into the reservoir is to reduce the interfacial tension between the crude oil and the displacing fluid in order to increase the capillary number and displace oil. During alkaline injection, the surfactant is generated in the reservoir when the alkaline substances that react with the acid components of the crude oil are used; for this reason, the alkaline injection is preferred in reservoirs of heavy and extraheavy oil [32]. Polymer injection looks to increase the viscosity of the displacing fluid to achieve an optimal mobility ratio that allows a greater sweep of crude oil in the reservoir [33]. In some cases , such as in ASP injection (alkali-surfactant-polymer) and SP injection (surfactant-polymer) [32, 34], various substances are combined.

1.3 Enhanced Oil Recovery Methods by surfactant injection

Surfactant injection has been a widely used and studied chemical recovery method, particularly in recent decades [3]. The surfactant plays an important role when contacting the reservoir, in addition to decreasing the interfacial tension between the crude and the displacing fluid can also change the wettability of the medium, allowing the oil detachment due to the decrease in capillary forces.

Knowing the chemical nature of the surfactant is of great importance in predicting the performance of these substances in recovery processes. The interactions that surfactants may have with fluids or rock in the reservoir can significantly affect the recovery process. The adsorption of this material in the rock and the non-interaction with the crude oil front can economically affect the process. Also, the formation of emulsions plays an important role [3, 4]. The application of this method is limited by a technical evaluation where the interaction between the phases involved is verified. This evaluation has traditionally been carried out in a core injection test [4, 6], although there is a growing trend in the use of microfluidic devices for the evaluation of these processes [7, 14, 35-38].

1.4 Microfluidic devices for the CEOR Processes evaluation by surfactant injection

Micromodels are devices designed to replicate the porous medium in order to analyze in detail the processes that occur at the pore scale. Due to the characteristic length of these devices, which is similar to that of oil-bearing rocks ($1x10^{-6}$ m -$1x10^{-9}$ m), they can be used to understand the processes that control oil extraction..

Micromodels can be designed with different materials such as glass, quartz, polymer, or silicone. They can also be etched with different patterns that can be classified as perfectly regular, partially regular, fractal patterns and irregular patterns. [9, 15, 18].

Since the design of the first micromodel in 1952 [39], consisting of a monolayer of glass spheres positioned between two flat glass plates and which was used to visualize the behavior of fluids in a porous medium, the techniques to define and design micromodels have evolved. Due to the visualization problems between phases present in the first micromodels caused by little differentiation of refractive index, the design of new micromodels with regular geometries began [40].

Perfectly regular micromodels are those that have all the pores with the same geometry, width, and depth [9, 40]. An example of this type of micromodel is shown in Figure 1.

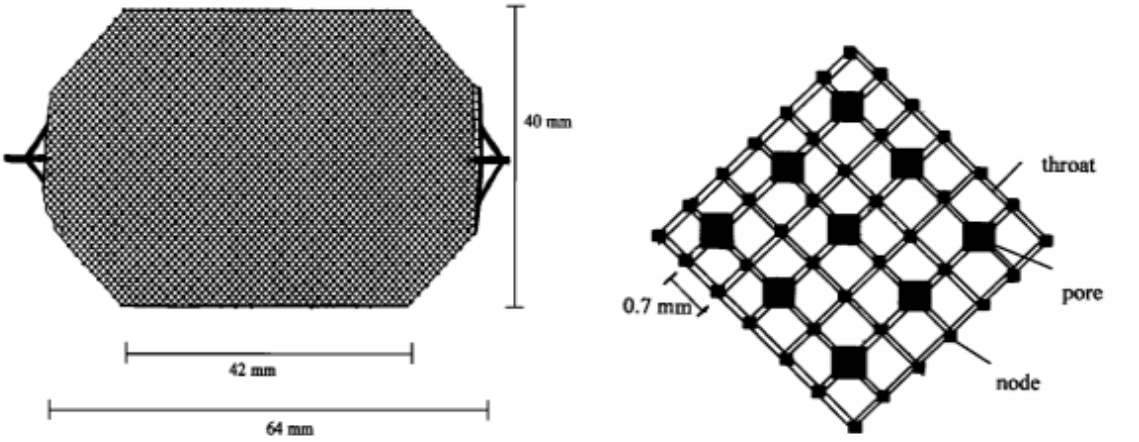

Figure 1. Micromodels with perfectly regular geometry [41]

Partially regular micromodels have a regular network with pores of the same cross-section, but unlike the previous ones, the pore size in these micromodels is variable. The sizes of the different pores present in these types of micromodels can be correlated from a statistical distribution [9]. An example of partially regular micromodels is shown in Figure 2.

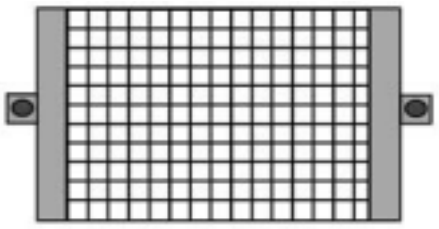

Figure 2. Micromodel with partially regular geometry [42]

Fractal pattern micromodels are designed from repeating figure patterns forming a correlated configuration based on fractal theory [43]. Due to the shapes that nature presents, this theory helps to represent rock patterns more simply [9]. An example of a fractal pattern micro-model is shown in Figure 3.

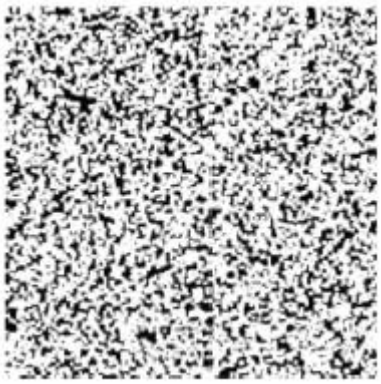

Figure 3. Micromodel with fractal pattern geometry [44]

Irregularly patterned micromodels have uncorrelated pores with spacing and random shape. The size of each pore can be taken from one or more statistical distributions [9]. An example of this type of micro-model is shown in Figure 4.

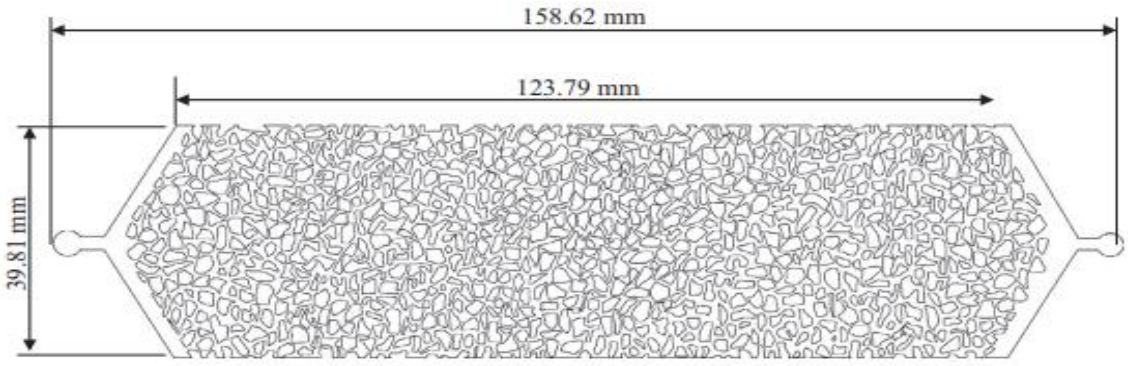

Figure 4. Micromodel with irregular pattern geometry [45]

In the manufacture of the microfluidic devices, depending on the micromodel type to be designed, the desired pattern, and the type of material used, there are several methods. Some of the most important manufacturing methods are mentioned below. These have been extensively analyzed in the specialized literature on the subject due to their current use [9, 20, 40, 46, 47].

The first micromodel manufacturing process appeared in 1952 with the use of spheres between plates [9, 39]. These micromodels have a fluid inlet at the center [48] or at the ends of the device [49]. The micromodels made from this technique are easy to fabricate

however they present problems with the visual evaluation of the fluids inside the devices, especially around the large size spheres.

Another manufacturing method is optical lithography or photolithography, in which a flow pattern has already been predesigned along with design characteristics, and a gall photosensitive plate is used for etching. The production cost for this manufacturing method is inexpensive and is widely used to create irregular or fractal-pattern micromodels [44]. This manufacturing method uses heating of the glass plate and UV exposure to etch the flow pattern on the plate.

The micromodel etching method is based on chemical reactions and the interaction of laser and radiation with glass or polymer. This method can be divided into two techniques: wet etching, where chemicals are used to etch the flow pattern on the plate [50]. The second technique is named plasma or laser etching, where electromagnetic radiation is used for engraving the desired flow pattern [51].

Stereolithography is a computer-based method of manufacturing micromodels [52]. In this technique, flow patterns can be designed from computer-aided design. The manufacture of micromodels is based on the controlled solidification of a liquid resin by photopolymerization.

Finally, soft lithography collects the manufacturing methods to obtain micromodels using soft or easily malleable materials. Soft lithography is generally used to design small or simple geometries on the micro and nanoscales [53].

As previously mentioned, an advantage of using micromodels is the phase displacement visualization within these devices. The results taken from the tests carried out on micromodels are based on image analysis. Visualization of the processes that occur within the micromodels can be carried out through different methods: microscope, microscope with a camera, photoluminescent volumetric method, and fluorescent microscopy [9].

The direct visualization with a camera allows taking different images of the micromodels, where sometimes it is necessary to use lenses that allow taking the necessary detail [54].

The use of a microscope facilitates the work of specifying areas of interest within the device, but sometimes does not allow full coverage of the camera, leaving it motionless at the same point [55]. The photoluminescent volumetric method uses fluorescent substances to be located at the interface of the fluids, so that later, through a laser, the interface can be illuminated. In this way, the image can be captured [56].

1.5 Micromodels properties.

Micromodels are an efficient tool for evaluating different fluid displacement mechanisms in porous media [9]. These devices have been widely used to assess CEOR technologies, comparing different scenarios and describing phenomena that allow the mobility of crude oil in the porous medium. The possibility of changing geometric characteristics in the design of the micromodels allows to quickly evaluate oil recovery methods.

Due to the easy manipulation of geometric and physical characteristics in the micromodels, these can reflect the change of different petrophysical properties that characterize a reservoir and affect the EOR processes. In this way, microfluidics is an easy-to-use tool, where the times and spaces involved in the analyzes are shorter, making the evaluation of crude oil displacement processes, particularly CEOR processes, more efficient.

Given the inherent complexity of the oil reservoir, evaluation of the design parameters of micromodels is required when evaluation the effect of surfactant injection as a CEOR processes. The effect of geometric parameters of the porous media have been evaluated [27, 57-59] to assess their influence on the oil displacement processes. The evaluative process has been carried out experimentally and by simulation, allowing to characterize some flow patterns according to a given geometry and the fluids used for the displacement.

Some of the variables analyzed by simulation in computational fluid dynamics have been the pore shape and distribution in terms of the connectivity between pore and pore throat, heterogeneity, and tortuosity [27]. Geometric characteristics, such as the presence of fractures, have been experimentally evaluated, including the degree of orientation of fracture with respect to the injection point and the spacing between them. Research carried

out has demonstrated the importance of each of these characteristics and their influence on the responses of the tests carried out on micromodels [58].

Some variables that has been studied in microfluidic devices are: Porosity, that define the pore fraction of the geometry, it indicates the interconnected space available for fluid interaction [27, 60]. Grain shape, that affects the amount of crude oil that interact with the micromodel surface, making the surface phenomena, as wettability, important in displacement processes [27, 61]. Presence of fracture, that influences in the displacement process performance, it affects breakthrough time and fluid distribution within micromodels [13, 32, 35, 58]. Fracture configuration in terms of orientation, width, length can modify recovery factor as well as breakthrough time and fluid distribution in micromodels [13, 35, 58]. Heterogeneity that affects the pore size distribution and relates the performance of displacement processes with fingering effect [27, 62, 63]. Tortuosity that relates the flow path in a displacement process with the distance between two points, this property affects the breakthrough time and recovery factor [27]. Injection velocity that affects the relation between viscous and surfaces forces, in this way, a change in velocity could make an easier displacement or channel the displacing fluid [28]. Pore shape that allows visualizing the fluid displacement and the way the fluids interact, as the grain shape, the pore shape plays an important role in the relation between the fluids and the micromodel wettability [27, 61]. Pore-throat connectivity that affects the flow and shape of the displacing fluid, allowing interactions crude oil/displacing fluid/micromodel material that modify the amount of crude oil trapped inside the porous of a micromodel [27].

In this research, the grain shape, injection velocity, presence of fracture and porosity are considered as the micromodels properties to analyze. These properties are chosen due to their influence on the surfactant injection processes, where the modification of these properties allows to observe evidence of changes in responses of interest such as the recovery factor or determining the displacement performance in terms of the interdigitation effect or the amount of crude oil that adheres to the walls of the micromodel. In addition, the easy manipulation of these properties in micromodelos allows to modify them through computational drawing tools.

The following section describes the properties considered in this research, and their relation with the petrophysical properties that characterize a reservoir is made.

1.5.1 Grain shape

The effect of pore shape in the micromodels has been previously studied [27, 64] to analyze the entrapment effect on the oil recovery process. These studies found that, at the microscopic level, micromodels with pores that have corners, such as square or triangular figures, are more suitable for studying entrapment in porous media and that the flow of the displacing fluid along with the amount of residual oil strongly depends on the pore size and distribution [27].

It is known [27, 65] that, by changing the connectivity between the pores and the randomness by which they are distributed within the microfluidic device, the porous media configuration can resemble the arrangements of pores in a reservoir only. Changes in grain size can be targeted to represent changes in the tortuosity of the medium, providing a more significant similarity to that required in a field.

The shape and pore distribution within a microfluidic device affect the porosity, permeability, and tortuosity of the porous medium. The latter are properties that directly affect the recovery processes. Out of the multiple possibilities for pore shape and distribution, this research considered only circular and irregular shapes as these two present different interactions that the fluids have at a microscopic level when they are inside a pore. In this way, when the micromodel contains grains with a circular shape, the displacement of the fluids that are wettable to the medium is facilitated, because of the absence of corners and vertices that increase the adhesion forces of the wetting fluid. [66-68]. On the other hand, On the other hand, the irregular shape of the grain does not allow the displacement of the crude oil as easily as in the circular grain, since it presents corners or spaces that are difficult to access. The irregular shape of the grain makes it possible to evaluate other aspects in the crude oil displacement processes considering different access points to the crude oil that is trapped in the porous medium. [59]. the distribution considered for this research is a random distribution of the grains, this choice is made based on the information presented in the specialized literature on the subject where they indicate that this type of

distribution resembles that of an oil deposit where the oil displacement processes take place [27, 41, 69, 70].

1.5.2 Injection velocity

The important of the injection velocity influences on CEOR processes is well documented [59, 68], therefore the selection of this parameter for the analysis of their influence in the micromodel performance is straightforward. The injection velocity has a significant influence on the recovery factor at the breakthrough time [28].

1.5.3 Presence of fractures

The presence of fractures in reservoirs increases permeability as well as porosity and reducing the tortuosity of the porous medium.

The way fractures occur significantly affects the oil recovery processes depending on the fluids present in the porous medium and the interaction between them [58]. The fracture can serve as a conduit for the wettable phase to move quickly, reducing pressure drop or distributing fluids in the porous medium. Likewise, fractures can lead to natural channeling and low oil recovery. This variable can easily be modified in the design stage of a micromodel.

Experimental characteristics have been analyzed to improve understanding of the presence of fractures on microfluidic devices [58]. Results have shown that many characteristics affect EOR processes, such as the relationship between fracture length and width, fracture position within the micromodel, the angle of inclination, and the number of fractures. This study only considers the effect of a fracture positioned in the center of the micromodel at an angle of 45 ° with respect to the displacement direction. This configuration was selected because it has shown, through research, that it helps to obtain a greater recovery factor, that is, this configuration makes it easier for the displacing fluid to move easily to occupy a larger space within the micromodel, in addition to facilitating contact between phases.[35, 58].

1.5.4 Porosity

Porosity is one of the physical properties of the porous medium and is of great importance for the study of CEOR processes in micromodels. Porosity is defined as the ratio of the pore volume to the total volume of the rock [71]. Porosity is classified as absolute, which considers the entire porous volume of the rock; effective, which considers only the interconnected porosity; and non-effective, which is the difference between absolute and effective porosity. The micromodels analyzed in this work were designed with interconnected pores, and the chosen porosity ranges from 0.5 to 0.7 because this is the most frequent configuration found in the revised literature [9, 15, 21-23, 32, 35, 46, 65, 72-75]. Typical porosity values in reservoirs range from 0.17 to 0.5 [76, 77] which are lower than those used in micromodels, to guarantee proper flow visualization in micromodels, high porosity values are preferred [10, 78]. The understanding in the micromodel community is that the conclusions of the flow pattern, obtained at the higher porosity range can be extended in the porosity values in the field [9, 10, 41].

1.6 CEOR processes simulation in microfluidic devices through CFD

CFD has been frequently used to simulate multiphase flow in micromodels, particularly in EOR processes [21, 27, 57, 61, 64, 65, 70, 79, 80]. Different characteristics are evaluated to optimize and characterize the recovery processes in a short time with the use of a computer. In a 2015 study, Gharibshahi [27] evaluated the effect of pore morphology, distribution, heterogeneity, shape, and tortuosity of different micromodels using CFD. and found that the use of a random distribution of grain within micromodels has better adjustments to the experimental data.

In 2019 Minakoy et al. [80] investigated the effect of nanoparticle addition in a displacing fluid through CFD simulations and micromodel experiments. They observed that the use of nanoparticles increases the oil recovery factor and explained this behavior by improvement of rock wetting, in this study the CFD simulation complemented the experimental work. Finally, Rostami et al. [57] studied through CFD simulations in a micromodel the change of wettability of a porous media in a EOR process. They were able to use CFD simulations to

explain the phenomena observed through microfluidics experiments and justify the increase of the recovery factor in the micromodels due to changes in wettability.

In addition to studying the morphological aspects of micromodels for EOR processes using CFD simulations, fluid interactions in the porous medium of micromodels have also been studied. The displacement of crude oil with biosurfactants has been analyzed through CFD simulations of micromodels [61, 65] , the results have shown an improvement in the oil recovery factor and a decrease in the interdigitation effect, this was done in micromodels with different grain shapes, such as square and circular, with random pore distributions. Also, modifications in the displacement fluid have been evaluated in CFD simulations of micromodels [57, 80], in these, the addition of new components such as nanoparticles change the properties of fluids such as interfacial tension and viscosity, which increases the recovery factor and allows an uniform distribution of displacing fluid in the micromodel. The latest investigations were conducted in order to gain a better understanding of EOR processes, also demonstrating the use of CFD simulations as a tool to evaluate such processes when nanoparticles are used for fluid modification.

From the aforementioned investigation, CFD technique is presented as an instrument for evaluating CEOR processes by simulating micromodels.

1.7 Mathematical modeling

This section describes the mathematical modeling along with the description of the software used to solve the proposed equations and the validation of the model based on the experimental data taken from [28].

1.7.1 ANSYS Fluent 19.1

ANSYS Fluent 19.1 is a commercial software used to model fluid flow. This software can represent transport phenomena through a large number of mathematical models that adjust to different set of conditions, including complex geometries according to the user's needs [81].

The CFD technique solves the conservation equations through the finite volume method, which is generally described as follows [26]:

- Approximation of the geometric domain to be studied in control volumes.
- Representation of conservation equations in an integral form for each control volume.
- Discretization of the integral form of the conservation equations to obtain an algebraic system of equations.
- Definition of boundary conditions and inclusion in an algebraic system of equations.
- A solution of an algebraic system of equations through iterative methods.

1.7.2 Mathematical description

In this section, equations that govern fluid flow within micromodels will be described. Considering that temperature is constant, the energy conservation equation is not considered in this investigation. Thus, the problem can be mathematically defined by the conservation of mass and momentum equations.

Considering a Eulerian approach, where a control volume is taken for the description of the conservation equations, and that the micromodels in the simulations are considered 2D geometries due to their low depth compared to the others dimensions [22, 27, 61, 65], the mass conservation equation is described as shown in Equation (1.1).

$$\frac{\partial \rho}{\partial t} + \nabla \cdot (\rho \vec{u}) = 0 \tag{1.1}$$

where $\vec{u} = (u, v)$ is the velocity vector, and ρ is the fluid volume-averaged density, which is considered constant due to the low compressibility of the treated fluids.

The momentum conservation equation is described through the vector notation in Equation (1.2).

$$\frac{\partial (\rho \vec{u})}{\partial t} + \nabla \cdot (\rho \vec{u} \vec{u}) = -\nabla p + \nabla \cdot [\mu (\nabla \vec{u} + \nabla \vec{u}^T)] + \vec{F} \tag{1.2}$$

where p is the pressure, μ the dynamic viscosity coefficient and $\vec{F}$ is the surface tension force. As can be seen in the conservation of momentum equation, gravitational forces were not considered for the development of this investigation.

To describe the multiphase flow within the micromodels, the VOF (volume of fluid) model incorporated in Ansys Fluent is used to track the interface between the oil and the displacing fluid. This model calculates the volumetric fraction of each of the phases within each cell in the domain [81]. Equation (1.3) describes the tracking of the interface through the volume fraction of phases i and j.

$$\frac{1}{\rho_i}\left[\frac{\partial(\alpha_i\rho_i)}{\partial t} + \nabla\cdot(\alpha_i\rho_i\vec{u}_i) = S_{\alpha i} + \sum_{j=1}^{n}\left(\dot{m}_{ji} - \dot{m}_{ij}\right)\right] \quad (1.3)$$

where $\dot{m}_{ji}$ y $\dot{m}_{ij}$ are mass transferred between phases i and j, $S_{\alpha i}$ is the source term of phase i, ρ_i is the density of phase i, $\vec{u}_i$ is the velocity vector for phase i and α_i is the volume fraction of phase i. The phases within the micromodel are considered as immiscible, due to this the values of $\dot{m}_{ji}$ and $\dot{m}_{ij}$ are zero. The volume fraction α_i can be defined as follows.

- $\alpha_i = 0$: the cell is empty.
- $0 < \alpha_i < 1$: the interface is located in the cell.
- $\alpha_i = 1$: the cell is filled with phase i.

The sum of the volumetric fractions of each phase within the cells analyzed must be one.

$$\sum_{i=1}^{n}\alpha_i = 1 \quad (1.4)$$

In a system that only contains two phases, if a cell is entirely occupied by phase i, the cell will have the properties of this phase, but if a cell is occupied by two phases ($0 < \alpha_i < 1$), properties taken by this cell will be a mixture of the properties of the two phases weighted by the volume fraction of each of the phases.

$$\rho = \alpha_i\rho_i + (1-\alpha_i)\rho_j \quad (1.5)$$

$$\mu = \alpha_i \mu_i + (1 - \alpha_i)\mu_j \tag{1.6}$$

where ρ y μ are the density and viscosity in the cells occupied by two phases, respectively.

It is necessary to calculate the surface forces to solve the equations. This is done through the continuum surface force model (CSF) [82]. The surface tension force is calculated as shown in Equation (1.7)

$$\vec{F} = \sigma_{ij} \frac{\rho \kappa_i \nabla \alpha_i}{\frac{1}{2}(\rho_i + \rho_j)} \tag{1.7}$$

where σ_{ij} is the coefficient of surface tension and κ_i is the curvature of the interface taken from inside the phase i. κ_i is defined in terms of the divergence of the unit vector of the phase i fraction gradient.

$$n = \nabla \alpha_i \tag{1.8}$$

$$\kappa_i = \nabla \cdot \hat{n} \tag{1.9}$$

where n is the normal vector to the interface surface and $\hat{n}$ is the unit vector. The phase wettability is used employing the contact angle to adjust the interface curvature in areas close to the walls of the micromodel.

$$\hat{n} = \hat{n}_w \cos\theta_i + \hat{t}_w \sin\theta_i \tag{1.10}$$

where $\hat{n}_w$ y $\hat{t}_w$ are the unit vectors normal and tangential to the wall of the micromodel and θ_i is the contact angle of phase i with the wall of the micromodel.

The multiphase model focuses on interface analysis; knowing how the treatment is close to this area is of great importance for this investigation. Interpolation close to the interface is performed with geometric reconstruction. Figure 5 shows the reconstruction of the interface using this method.

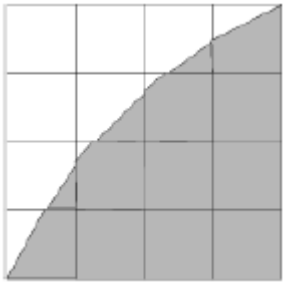

Figure 5. Interface shape represented by the geometric reconstruction (piecewise-linear) scheme [81] .

The geometric reconstruction scheme represents the interface between fluid using a piecewise-linear approach. It assumes that the interface between two fluids has a linear slope within each cell. For calculation of the advection of fluid through the cell faces uses linear shape. This scheme was selected because is the most accurate for general unstructured meshes. The reconstruction consists in three steps: The first calculates the position of the interface relative to the center of each cell. The second step calculates the advecting amount of fluid in each face through linear interface representation. The las step calculates the volume fraction in each cell [81].

2. Use of a Selection Flowchart for the Design of Micromodels for the Evaluation of Surfactant Injection in Enhanced Oil Recovery Processes through CFD simulations

Abstract

The evaluation of the factors that affect the CEOR process with surfactant injection is a complicated task; knowing how to improve this process is of great interest to the oil and gas industry. The aim of this study was to analyze the effect of different surfactants in the ultra-low interfacial tension range in microfluidic devices through CFD simulations in order to be able to evaluate different parameters and use a selection flowchart for microfluidic devices in CEOR processes with surfactant injection. A characterization of modifiable variables in micromodels is performed along with the type of response variables that can be obtained from the surfactant injection processes. In addition, a relation is made between these variables from information found in the literature. A selection flow chart is presented detailing the procedures for the choice of micromodels and is implemented through CFD simulation. The characteristics evaluated in micromodels were porosity (0.5 -0.7), grain shape (circular – irregular), presence of fracture and injection velocity (10 ft/day– 30 ft/day).

The response variables in the injection process in the micromodel were the recovery factor, breakthrough time, fractal dimension of flow patterns, pressure drop, and entrapment effect. For interpretation of the relations between the response variables and the modified variables, factorial experimental design analysis was used. The application of the selection flowchart through CFD simulations allows to identify a micromodel with geometric characteristics that differentiates the performance between two surfactants with similar properties. The obtained micromodel has a porosity of 0.5, with a circular grain shape and the presence of fracture, in addition, it must be operated with the maximum injection velocity (30 ft/day). The procedure developed in this research will facilitate the design of micromodels by coupling this technology with CFD simulation techniques.

Keyword: Computational fluid dynamics simulations; Chemical Enhanced Oil Recovery; Microfluidics

1. Introduction

With the development of modern life and global energy demand, the supply of resources such as oil continues to be necessary and vital. In oil extraction processes due to capillary forces, a large amount of oil is trapped in the reservoir that must be extracted by other methods. Currently, Enhanced Oil Recovery (EOR) methods are used to substantially improve oil production [30]. One of the best known EOR methods is the injection of surfactants, this reduces interfacial tension between the oil and the displacement fluid, increasing the capillary number, allowing that the crude oil separates from the reservoir walls, and increasing the oil recovery factor

Surfactant injection is a Chemical Enhanced Oil recovery (CEOR) technique with easy application and great potential [83]. Among available approaches to evaluate surfactant injection, microfluidic devices have been used due to their visible porous media that allow the interrogation of the fluid pattern. Microfluidic devices are an excellent alternative to core injection tests because they demand a shorter evaluation time and their aforementioned availability for visual characterization of the flow at the pore level [11]. Micromodels can be fabricated of different materials such as glass, quartz, silicon, or polymers. The porous

media geometry in micromodels can take different forms: perfectly regular, partially regular, fractal, and irregular. The geometry of a micromodel device can even be that of a reservoir prototype by taking a scanning electron microscopy (SEM) images from a reservoir rock. Fabrication methods for micromodels are optical lithography, etching, stereolithography, and soft lithography [8, 10, 17, 18, 84].

CFD is used to study systems that involve fluid flow, heat transfer, among other phenomena through computer-solved algorithms [26]. CFD solves the conservation equations by discretization of the computational domain. CFD simulations of micromodels have been used to evaluate the effect of pore morphology and size-distribution in terms of pore-throat connectivity, heterogeneity, shape and tortuosity [27] on the micromodel performance when evaluating the result of changes of temperature, viscosity, density, and the interfacial tension of surfactants [57, 70, 79]. Particularly, Gharibshahi et al. [27] evaluated the effect of pore morphology for EOR processes in micromodels using CFD. They concluded that the fluid flow in the randomly-distributed porous medium closely resembles the fluid flow in reservoirs. Jafari et al. [65] analyzed the effect of biosurfactants in EOR processes through CFD simulations. In this investigation, a micromodel was used to determine that the recovery factor increases and the interdigitation decreased after the sues of the biosurfactant shown. Similar results were obtained by Mohammadi et al. [61] when they simulated the oil displacement process in a micromodel with quadratic pore shape using as displacement fluid a surfactant obtained from the Zyziphus spinachristi tree. Rostami et al. [57] experimentally and through CFD simulations evaluated the effect of displacing fluid modification on EOR processes. Similarly, through CFD simulations, Minakov et al. [80] evaluated the effect of modifications of displacing fluids with nanoparticles in EOR processes in micromodels.

While all these previous studies presented good evidence of the possibility of modelling the flow in microfluidic devices, the refereed literature does not present any study that attempted to use CFD to define key geometric parameters and experimental conditions of a microfluidic test that could better allow for the detection of differences in the performance of surfactants in the ultra-low interfacial tension range ($< 10^{-2}$ mN/m).

.

A micromodel selection flowchart that would render the best configuration for the evaluation of the performance of surfactant injection in CEOR process is something very much

desirable as it would save time and reduce experimental cost. This chapter describe the construction of one of such flowcharts. Firstly, micromodels used for the analysis of the surfactant-injection processes are characterized in order to generate typical geometries that could be modelled with CFD. After running thirty two different CFD simulations that resulted from a factorial design of the combination of microfluidic geometrical characteristic as well as process conditions, a simple sensitivity analysis was carried out in order to propose a flowchart that can be followed in order to determine the micromodel that allows to better differentiate the performance of various surfactants.

2. Towards a micromodel selection flowchart

This section describes the procedures implemented to create a selection flowchart for micromodels used for CEOR processes with surfactant injection. First, the relations between the modifiable variables within the operation in a micromodel and the response variables obtained from these devices are described. In addition, a methodology for the identification of the response variables that are most affected by the use of different surfactants is described.

2.1 Description of variables in a micromodel for CEOR processes with surfactant injection

Microfluidic devices can be used to evaluate multiple factors that affect the CEOR processes.

Table 1 shows a compilation of the variables that can be modified in a micromodel along with a brief description as well as examples of studies where these variables have been analyzed.

Table 1. Modifiable variables in micromodels for CEOR processes

Modifiable variables in micromodels (X)	Description	References
Porosity	Indicates the amount of space within the micromodel available for the fluids to interact	[27, 60]
Grain shape	Affects the amount of oil that can get trapped due to adhesion to the medium	[27, 61]
Presence of fracture	Fractures can channel fluids, change breakthrough times and modify fluid distribution	[13, 32, 35, 58]
Fracture configuration	The orientation, width and length of the fractures affect the performance in terms of recovery factor and fluid distribution	[13, 35, 58]
Heterogeneity	Describes the distribution of the different pore sizes found in a micromodel. It is related to the fingering effect.	[27, 62, 63]
Tortuosity	The way the fluid direction is found. This directly affects the recovery factor.	[27]
Injection velocity	Defines the interaction of the viscous forces inside the porous medium	[28]
Pore shape	Characterizes the way in which fluids interact within a pore and how the wetting effect of the medium affects the flow distribution of these fluids	[27, 61]
Pore-throat connectivity	Relates to the connectivity of the pores. It directly affects the flow within the micromodels, in addition to the amount of crude that can get trapped inside the pores	[27]

Changes on the variables shown in Table 1 influence the performance of the processes evaluated in micromodels. The performance of surfactants can be evaluated in different ways, where the one of greatest interest is the recovery factor. On the other hand, when looking for different effects with the application of surfactants, it is of interest to evaluate properties such as the distribution of fluids within the porous medium, or the time required

for the displacement fluid to reach the outlet point of the porous medium. In this way, from the visualization of the fluids and the short experimentation time, the microfluidic devices allow the performance of surfactants to be evaluated with different parameters. Table 2 presents the type of response variables that can be obtained when using micromodels in recovery processes, also shows previous investigations where these variables have been investigated.

Table 2. Response variables evaluated in micromodels for CEOR processes.

Response variables in micromodels (Y)	Characteristic	References
Recovery factor	it has been investigated in different micro-models, from capillary type to complete porous media	[27, 61, 65, 66, 68, 70, 79, 85]
Pressure drop	It has been calculated based on the pressure drop in a porous medium or through an interface with representations of capillaries	[67, 68, 86]
Fractal dimension	Different types of micromodels have been investigated, although in recent years this variable has not been continuously worked on.	[87, 88]
Breakthrough time	It has been worked on micro models that represent completely porous media	[27]
Viscosity	The viscosity of the displacing fluid and the fluid when they leave the porous medium and the effect of other variables on this have been evaluated.	[70, 86]
Displacement micro mechanisms	These have been analyzed through microscopic observations or through numerical simulation in many types of micro-models.	[67, 68, 89]
Emulsion formation	Due to the visualization that micromodels allow, emulsion formation can be observed through microscopes	[90]
Drops shape	The way the drops take shape indicates the distribution of forces through an interface. This has been done through microscope visualization and numerical simulation.	[66, 68, 85, 89, 91]
Fluid distribution	one of the main advantages of the micromodels is the visualization of	[27, 61, 65-67, 70, 79, 85, 89]

the phases moving. For this reason, most of the research focuses on this topic.

A relation between the modifiable variables of a micromodel (X) shown in Table 1 and the variable responses (Y) shown in Table 2 is shown in Table 3. An intense gray indicates a strong relation while white implies almost no relation between both.

Table 3. Relation between modifiable variables and response variables of a micromodel

Y \ X	Porosity	Grain shape	Presence of fracture	Fracture configuration	Heterogeneity	Tortuosity	Injection velocity	Pore shape	Pore-throat connectivity
Oil recovery factor									
Pressure drop									
Fractal dimension									
Breakthrough time									
Viscosity									
Displacement micro mechanisms									
Emulsion formation									
Drops shape									
Fluid distribution									

In this way, if it is required to evaluate surfactants with the recovery factor as response variable, it is recommended to analyze the presence of fractures, injection velocity, and pore-throat connectivity in the micromodels. These are the modifiable variables that have a greater impact on the recovery factor (strong influence). Following the same approach used for the recovery factor, it is possible to evaluate the response variables to the surfactant injection processes in micromodels with the strongest influences related to the modifiable variables shown in Table 3. If the use of strong influences is not possible, it is recommended to use intermediate influences.

When it is necessary to evaluate multiple response variables, it is recommended to work with the combination of modifiable variables where the majority of strong and intermediate influences are obtained. Furthermore, if possible, that at least there is a strong influence combination for each response variable.

2.2 Methodology to evaluate the performance of surfactants in injection processes in micromodels

The relation between the modifiable variables of a micromodel (X) and the response variables of these devices (Y) is the criterion that allows evaluating the performance of surfactants. One way to evaluate this relation is shown in Figure 1, where the global methodology framed in this research is shown.

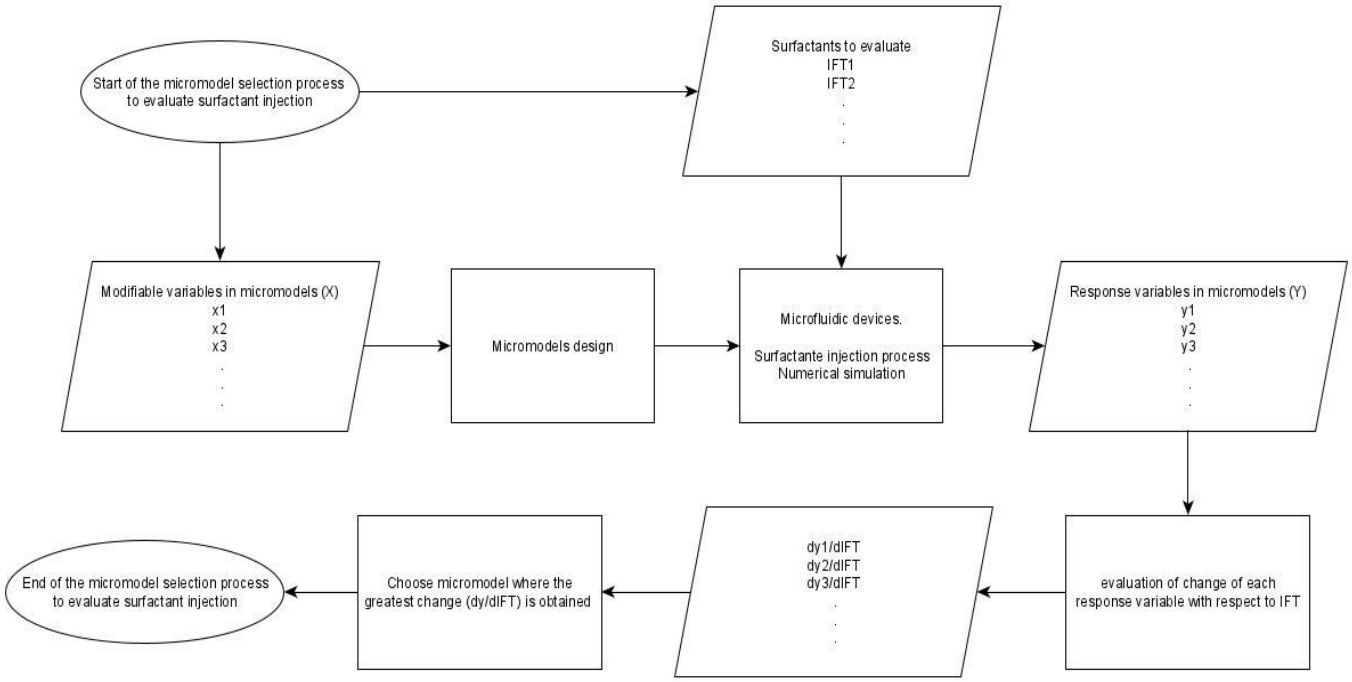

Figure 1. Flowchart to evaluate effect of surfactants on response variables (Y)

In Figure 1, the process starts with the selection of modifiable variables in micromodels (X) and with the surfactants to be evaluated in micromodels. Then, based on the chosen variables (X), the micromodels are designed. Subsequently, the surfactant injection processes are carried out and the response variables of the micromodels (Y) are evaluated. Then, the change of each response (Y) is evaluated with respect to each chosen surfactant through the interfacial tension (IFT) that these components have with the crude oil. Finally, these changes are classified and the case where the greatest change is obtained is

identified. The micromodel where the greatest change is obtained is the micromodel where the greatest difference between the surfactants evaluated can be seen.

The change of each response variable (Y) is evaluated through derivatives considering the number of displacement tests carried out for each considered micromodel. For this investigation, the following equation was used to evaluate the change of the selected responses variables (Y).

$$\frac{\mathrm{dY_1}}{\mathrm{dIFT}} = \frac{Y_{11} - Y_{12}}{IFT_1 - IFT_2} \quad (1)$$

where $\frac{\mathrm{dY_1}}{\mathrm{dIFT}}$ is the change of the variable Y, Y_{11} is the response variable in the micromodel 1 when using surfactant 1, Y_{12} is the response variable in the micromodel 1 when using surfactant 2, IFT_1 is the interfacial tension between Surfactant 1 and the crude oil, finally, IFT_2 is the interfacial tension between Surfactant 2 and the crude oil.

One way to obtain micromodels from the modifiable variables (X) is by making combinations of these variables. In this way, for example, using combinations of 3 variables in 2 levels, it is possible to obtain 8 micromodels. The number of variables that can be modified in a micromodel and the ability to evaluate each one will greatly affect the design of the micromodels.

For this research, the following response variables (Y) are taken for analysis. *Recovery factor*; It is the most analyzed variable in CEOR processes because this type of process is designed precisely so that this value can increase, this factor is the amount of crude oil that can be obtained from the displacement of fluid in a porous medium, generally reported as a percentage of the initial crude oil in the porous medium. *Breakthrough time*; it is the time it takes for the displacement flow to reach the outlet of the porous medium, this variable indicates how easily the displacement fluid can be channeled or can move through the porous medium. *Fractal dimension of flow pattern;* This variable allows quantifying the way the displacement front is distributed within the micromodel. The cases evaluated in this investigation are treated in 2D, which indicates that the fractal dimension will take values between 1 and 2, with a value closer to 2 being a mobility front with greater uniformity.

Pressure drop; it indicates the ease with which a fluid is going to move within the porous medium. In addition, it also relates the necessary energy that must be invested so that the process can take place. *Entrapment Effect;* It allows to quantify the amount of crude that is trapped or stuck to the grains of the porous medium due to interfacial forces, this accounting is only carried out to the areas where the surfactant could enter or contact the crude, for the areas of the porous medium where the surfactant did not contact, the calculation of the crude that remains trapped to the surfaces is not performed.

3. Numerical implementation

This section describes the software applied for the development of this research along with the calculation methods that include the description of the equations that model the process of surfactant injection within each of the micromodels. Also, the case design process for the micromodels evaluated in this research is described through experimental factorial design. In addition, a description is made of the creation of the geometries used for the CFD simulations along with its mesh and the mesh independence tests.

3.1 Simulation case design

To evaluate the different effects of the modified variables in micromodels, a two-level factorial experimental design with five factors (2^5 factorial design) was used [92]. The characteristics were labeled as grain shape (A), porosity (B), Injection velocity (C), presence of fracture (D), and Interfacial tension (IFT) (E). Characteristics range were selected from the available values in the literature. The two grain shapes were circular (-) and irregular (+); the former allows an ease detachment of crude oil compared to a quadratic or triangular shape, where, at the microscopic level, these are suitable for studying trapping effect in the porous media [27]. On the other hand, irregular pore shape is a better representation of the porous media of the reservoir [10, 22]. The minimum and maximum porosities were 0,5 (-) and 0,7 (+), respectively. Although this range is high when compared to the porosity in the reservoir, much of the research in microfluidics has been conducted within this range [9, 15, 21-23, 32, 35, 46, 65, 72-75]. The minimum and maximum injection velocities were 10 ft/day

(-) and 30 ft/day (+), respectively. The low-level injection velocity was chosen due to its use in research of microfluidics processes [21, 28, 37, 65]. Although a high level is a rare case in the research of microfluidic, it is of interest since it allows evaluating high velocities and their effect on the flow pattern [21]. The presence of fractures was coded as nonfractured (-) and fractured (+) micromodels; This characteristic allows the modification of response variables in micro models such as pressure drop, recovery factor and fractal dimension [13, 32, 58]. This research focused on the analysis of surfactant injection where ultra-low interfacial tensions are achieved, for this reason, the interfacial tensions evaluated were 0,037 mN/m (-) and 0,045 mN/m (+), the former is an experimental data obtained from [28], and the latter is a 20% larger value. The construction of the 2^5 factorial experimental design is shown in Table 4.

Table 4. The 2^5 factorial experimental design analysis along with the CFD simulation results

Grain shape	Porosity	Injection velocity (ft/day)	Presence of fracture	IFT (mN/m)	Breakthrough time (PVI)	Recovery factor	Fractal dimension	Pressure drop	entrapment effect
circular	0.5	10	nonfractured	0.037	0.4351	0.3882	1.5666	9.0840	0.0326
irregular	0.5	10	nonfractured	0.037	0.4069	0.3944	1.6281	42.1359	0.0429
circular	0.7	10	nonfractured	0.037	0.4112	0.3979	1.6610	3.5700	0.0411
irregular	0.7	10	nonfractured	0.037	0.4407	0.4100	1.7155	7.1765	0.0844
circular	0.5	30	nonfractured	0.037	0.4274	0.3800	1.5743	25.2136	0.0367
irregular	0.5	30	nonfractured	0.037	0.3829	0.3797	1.6428	117.325	0.0439
circular	0.7	30	nonfractured	0.037	0.3954	0.3832	1.6394	9.5758	0.0345
irregular	0.7	30	nonfractured	0.037	0.4476	0.4135	1.7102	19.2405	0.0974
circular	0.5	10	fractured	0.037	0.4227	0.3855	1.5880	9.4705	0.0579
irregular	0.5	10	fractured	0.037	0.3992	0.3785	1.6251	41.8144	0.0517
circular	0.7	10	fractured	0.037	0.4127	0.4027	1.6871	3.1050	0.0394
irregular	0.7	10	fractured	0.037	0.4426	0.4069	1.6933	6.7786	0.0788
circular	0.5	30	fractured	0.037	0.4031	0.3662	1.5834	26.1504	0.0151
irregular	0.5	30	fractured	0.037	0.3563	0.3390	1.6192	127.808	0.0708
circular	0.7	30	fractured	0.037	0.4245	0.4135	1.6763	8.6735	0.0554
irregular	0.7	30	fractured	0.037	0.4484	0.4093	1.7125	19.1542	0.1001
circular	0.5	10	nonfractured	0.045	0.4322	0.3861	1.5767	8.9602	0.0368
irregular	0.5	10	nonfractured	0.045	0.4392	0.4054	1.6229	42.6613	0.0491
circular	0.7	10	nonfractured	0.045	0.4045	0.3927	1.6627	3.5694	0.0408
irregular	0.7	10	nonfractured	0.045	0.4470	0.4178	1.7228	7.2455	0.0652
circular	0.5	30	nonfractured	0.045	0.4393	0.3906	1.5623	24.8362	0.0355
irregular	0.5	30	nonfractured	0.045	0.3705	0.3608	1.6484	119.187	0.0725
circular	0.7	30	nonfractured	0.045	0.4501	0.4325	1.6664	9.5706	0.0433
irregular	0.7	30	nonfractured	0.045	0.4257	0.3946	1.7056	20.9500	0.0935
circular	0.5	10	fractured	0.045	0.4306	0.3938	1.5859	9.3153	0.0640
irregular	0.5	10	fractured	0.045	0.3882	0.3702	1.6110	43.8324	0.0621
circular	0.7	10	fractured	0.045	0.4183	0.4079	1.6742	3.1890	0.0398
irregular	0.7	10	fractured	0.045	0.4468	0.4106	1.7297	7.0466	0.0766
circular	0.5	30	fractured	0.045	0.4075	0.3758	1.5831	26.0617	0.0757
irregular	0.5	30	fractured	0.045	0.3623	0.3457	1.6378	124.657	0.0558
circular	0.7	30	fractured	0.045	0.4303	0.4182	1.6680	8.7053	0.0528
irregular	0.7	30	fractured	0.045	0.4386	0.4031	1.7209	20.4482	0.0944

3.2 Geometry creation

In this study, different micromodels configurations were used to investigate the effect of different modifiable variables (X) such as *porosity*, *grain shape*, *presence of fracture*, and *injection velocity* in two different surfactant injection processes. Micromodels were considered two-dimensional geometries for the simulations due to their low depth compared to their other lengths [27, 70, 79]. The dimension of the micromodels porous media in all cases was 12.7 x 26.5 mm^2. Depending on the simulation, see Section 0, eight geometries were considered depending on porosity, grain type and the presence or absence of fractures. The geometries of the porous media were created using Matlab and CorelDraw. The process of creating each micromodel is explained below.

Micromodels with circular pore shape were obtained using Matlab to randomly distribute non-overlapping circles with a radius between 0.4-0.6 mm for porosities of 0.7 and radius between 0.5-0.7 mm for porosities of 0.5. Micromodels with irregular pore shape were obtained using CorelDraw software and information from the literature [28]; The non-fractured irregular model with an irregular pore shape is the same used in the experimental work with which the mathematical model of this investigation is validated [28]. the fractured micromodels have a preferential path in the center of the porous medium with an average width of 1.8 mm positioned at an angle of 45 ° with respect to the direction of the fluid. Figure 2 shows the geometries obtained. Also, Table 5 shows the properties of micromodels geometry.

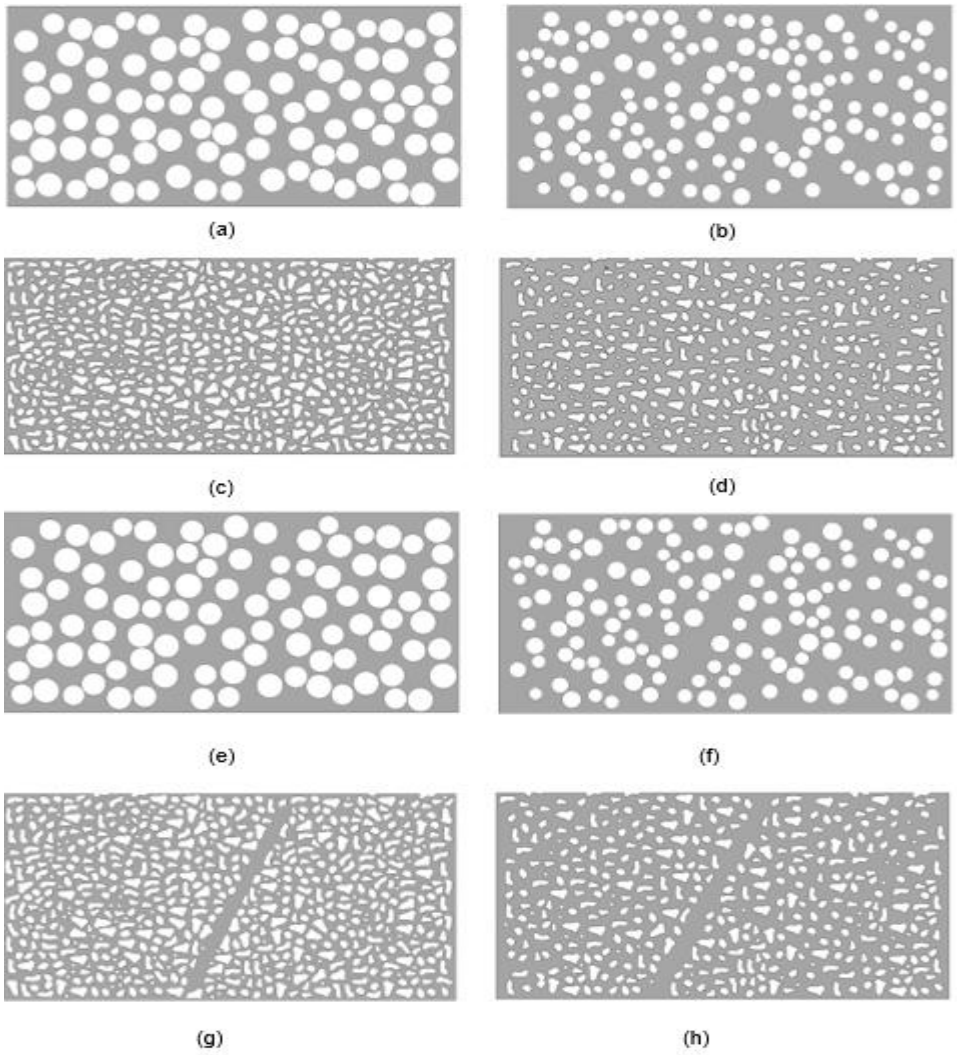

Figure 2. The schematic geometry of the designed micromodels.

Table 5. Physical properties of micromodels.

Micromodel	Grain shape	porosity	Presence of fracture
a	Circular	0.5	nonfractured
b	Circular	0.7	nonfractured
c	Irregular	0.5	nonfractured
d	Irregular	0.7	nonfractured
e	circular	0.5	fractured
f	circular	0.7	fractured
g	Irregular	0.5	fractured
h	Irregular	0.7	fractured

3.2.1 Meshing and grid independency check

Triangular unstructured mesh type was used for meshing the created geometries. For investigating the grid independency, grids with different number of elements were created. Then, for each grid, the governing equations were solved for water injection with a velocity inlet of 0.1 ft/day. The fluid pressure drops in micromodels were considered to compared grids. Equation (2) was used to calculate the relative error to compare the grids.

$$Error = \frac{|\Delta P_{Finer} - \Delta P_{Coarser}|}{\Delta P_{Finer}} \quad (2)$$

where ΔP_{Finer} and $\Delta P_{Coarser}$ are the pressure difference between the inlet and outlet with the finer mesh and coarser mesh, respectively. Table 6 shows the number of cells and nodes, the pressure drop, and the relative error for that are obtained in any grid. When the relative error between two consecutive grids is low enough that it can be neglected, the grid with a lower number of cells is selected as the grid for simulating the surfactant injection process. The number of cells for micromodels *a* to *h* are 178656, 146637, 411068, 324776, 155622, 218876, 408536, and 320726, respectively. Figure 3 shows the grid of micromodel D as an example. Appendix A shows the meshing of the geometries considered for this investigation.

Table 6. Pressure drop evaluated in micromodel grids.

Micromodel	Number of grid	Number of cells	Number of nodes	ΔP (Pa.)	Relative Error (%)
a	1	106232	82422	0.0175	
	2	178656	118890	0.0166	5.09
	3	683801	372377	0.0161	3.36
b	1	83248	51722	0.0068	
	2	146637	83689	0.0064	5.97
	3	379198	200661	0.0063	2.23
c	1	253863	143892	0.0954	
	2	411068	227317	0.0777	22.91
	3	1163110	617919	0.0761	1.97
d	1	134200	74919	0.0137	
	2	324776	175961	0.0128	7.25
	3	701344	36823	0.0127	0.48
e	1	94784	76642	0.0218	
	2	155622	107304	0.0186	17.07
	3	335658	197753	0.0179	4.17
f	1	106986	63755	0.0083	
	2	218876	120112	0.0074	12.15
	3	378635	200444	0.0070	5.84
g	1	252252	143061	0.0941	
	2	408536	226044	0.0807	16.63
	3	1169517	620897	0.0777	3.88
h	1	133312	74410	0.0150	
	2	320726	173874	0.0134	12.49
	3	694060	364896	0.0129	3.92

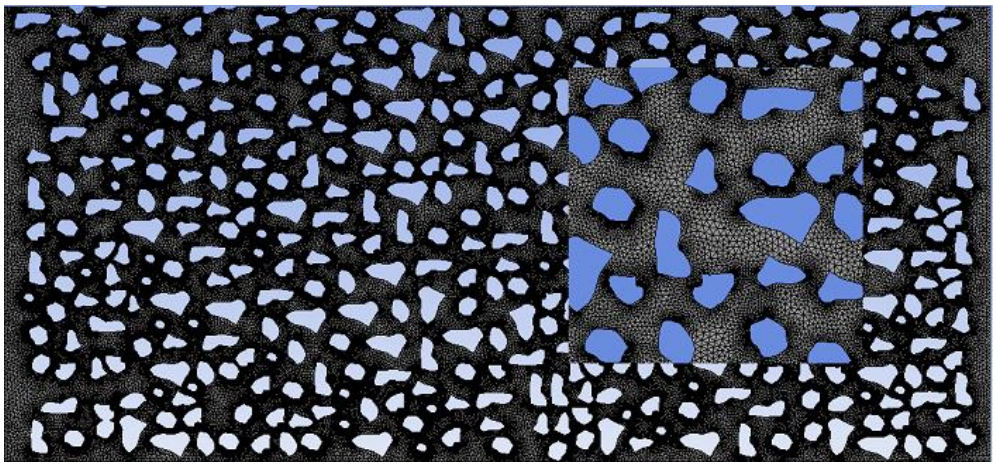

Figure 3. Meshing of the micromodel D geometry.

The quality of each of the meshes is evaluated through skewness. The results are shown in the following table.

Table 7. Mesh quality assessment from skewness value.

Micromodel	Maximum skewness	Average
a	0.96	0.28
b	0.98	0.11
c	0.73	0.095
d	0.75	0.085
e	0.96	0.24
f	0.98	0.095
g	0.93	0.0095
h	0.79	0.085

Skewness is defined as the difference between the shape of the cell and the shape of an equilateral cell of equivalent volume. Highly skewed cells can decrease accuracy and destabilize the solution [81]. From the results shown in Table 7, some meshes present a skewness value above 0.95, for this reason, it was reducing under-relaxation factor (Table 9) to avoid convergence difficulties

3.3 Operating conditions

The multiphase displacement processes within the micromodels are of great interest because different phenomena can be detailed, one of the most important stages is the breakthrough time, where the oil recovery begins to decrease and stabilize at a fixed value. This work focuses on the characterization of the CEOR processes in the micromodels at the breakthrough time. For this reason, all the results shown in this work are taken at the breakthrough time of the surfactant injection process, as was done in other investigations [9, 93].

For the characterization of the response variables in the CFD simulations carried out in this research, the following procedures were implemented. The oil recovery factor was obtained through the Area-weighted average of oil inside the micromodel calculated from Ansys Fluent, in this procedure, the quantity of a phase is quantified by dividing the sum of the product of the volumetric fraction of each phase and facet area in each cell by the total area

of the surface in the micromodel. Then, from this procedure the quantity of crude oil leaving the micromodel is quantified and compared with the quantity of crude oil at the beginning of the displacement process, in this way the recovery factor is calculated. The breakthrough time and the pressure drop were calculated from the numerical procedure applied in Ansys Fluent. For the fractal dimension of flow pattern at the breakthrough time, image analysis was used, where the fractal box counting method was applied to the images, and the fractal dimension was calculated. With the box counting method, the fractal dimension is obtained from the slope of the line of the plot of the logarithm of the number of boxes occupied by the pattern (N) and the logarithm of the inverse of the box size (r), in this way, D = log (N) / log (r), where D is the fractal dimension of the analyzed pattern. As an example, the fractal dimension obtained in Figure 4 is 1,66. For the entrapment effect, the proportion of area enclosed by the surfactant was calculated. As an example, Figure 5 shows in red color the proportion enclosed by surfactant (black). It is necessary to subtract the area of the grains from the indicated area for the calculation. The proportion of the entrapment effect in Figure 5 is 0.041.

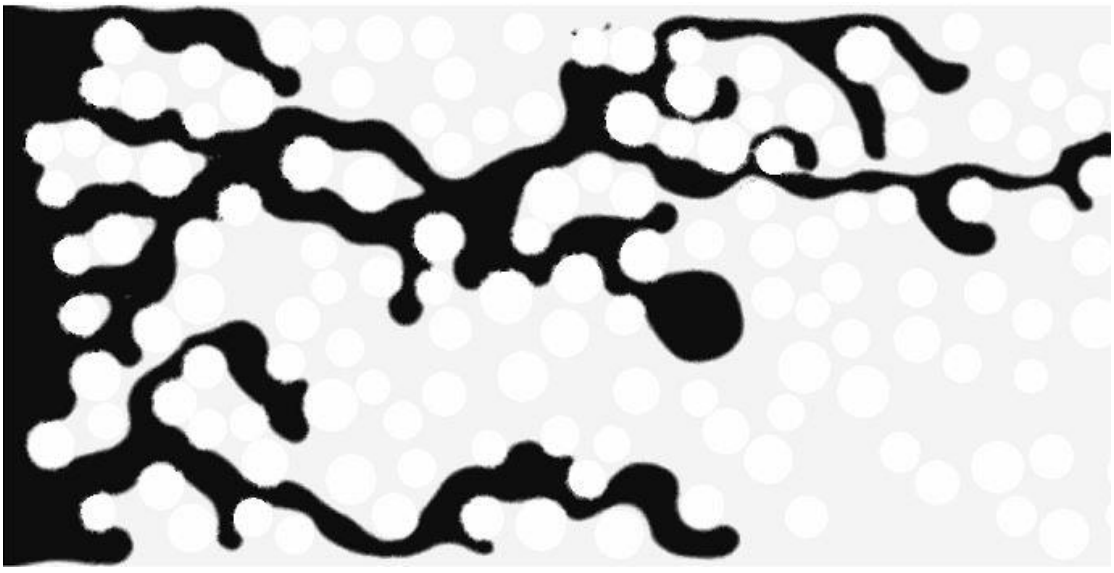

Figure 4. Flow pattern at the breakthrough time.

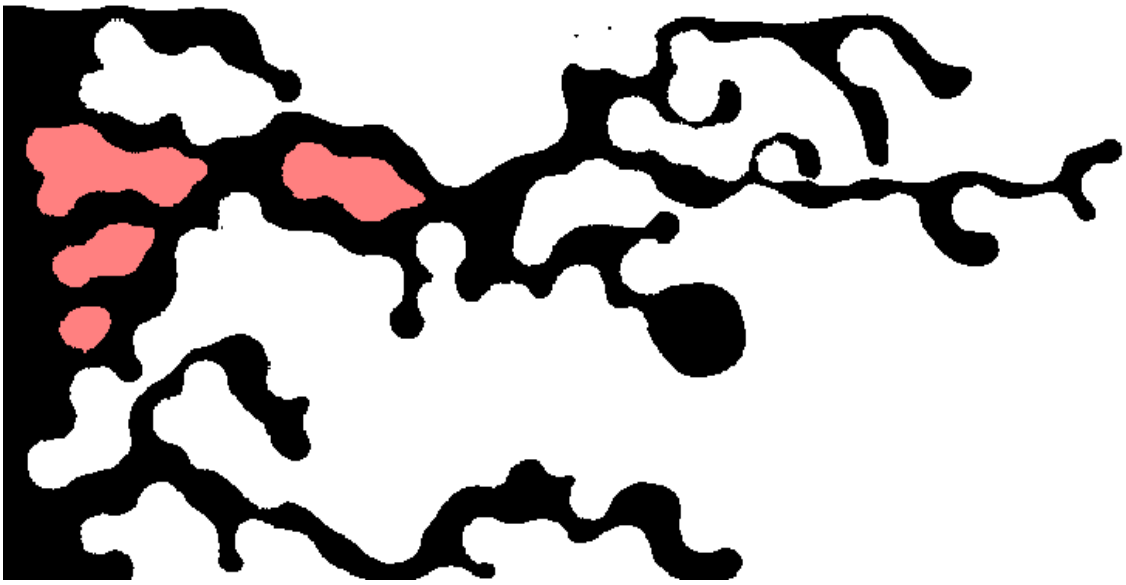

Figure 5. The entrapment effect in the micromodel.

3.3.1 Fluid properties

Table 8 shows the properties of the fluid in the simulation. Equation (3) shows the power-law for non-Newtonian viscosity that was used to adjust experimental data on fluid rheology.

$$\mu = \mathrm{k}\gamma^{n-1} \tag{3}$$

where μ is the apparent viscosity of the fluid, k is the consistency index, that is a measure of the average viscosity of the fluid, γ is the shear rate, and n is a measure of the deviation of the fluid from Newtonian.

Table 8. Properties of fluids.

Fluid	Density (kg/m^3)	k	n	Maximum viscosity (Pa.s)	Minimum viscosity (Pa.s)
Surfactant	1084.3	0.028	0.638	0.017	0.005
Oil	926.5	0.103	0.977	0.099	0.092

3.4 CFD Implementation

Ansys Fluent 19.1 software was used to solve the equations in this investigation applying the CFD technique. ANSYS Fluent is commercial software used to model fluid flow. This software can represent transport phenomena through a large number of mathematical models that adjust to different conditions [81].

3.4.1 Governing equations

In this investigation, a multiphase volume of fluid CFD model was used to simulate fluid flow in the micromodels [94]. The VOF (volume of fluid) is used to track the interface between the oil and the displacing fluid. This model calculates the volumetric fraction of each of the phases within each cell in the domain [81]. Also, this multiphase model considers the interfacial tension between phases and can be complemented with a contact angle value of one of the phases to describe the wettability of the medium. The relevant equations are as follows.

Continuity equation:

$$\frac{\partial \rho}{\partial t} + \nabla \cdot (\rho \vec{u}) = 0 \tag{4}$$

where $\vec{u} = (u, v)$ is the velocity vector, and ρ is the fluid volume-averaged density, which is considered constant due to the low compressibility of the fluids.

Momentum conservation:

$$\frac{\partial (\rho \vec{u})}{\partial t} + \nabla \cdot (\rho \vec{u} \vec{u}) = -\nabla p + \nabla \cdot [\mu (\nabla \vec{u} + \nabla \vec{u}^T)] + \vec{F} \tag{5}$$

where p is the pressure, μ the dynamic viscosity coefficient and $\vec{F}$ is the surface tension force.

Volume of fraction equation:

$$\frac{1}{\rho_i}\left[\frac{\partial(\alpha_i\rho_i)}{\partial t} + \nabla\cdot(\alpha_i\rho_i\vec{u}_i) = S_{\alpha i} + \sum_{j=1}^{n}\left(\dot{m}_{ji} - \dot{m}_{ij}\right)\right] \quad (6)$$

where $\dot{m}_{ji}$ y $\dot{m}_{ij}$ are mass transferred between phases i and j, $S_{\alpha i}$ is the source term of phase i, ρ_i is the density of phase i, $\vec{u}_i$ is the velocity vector for phase i and α_i is the volume fraction of phase i. The phases within the micromodel are considered as immiscible, due to this the values of $\dot{m}_{ji}$ and $\dot{m}_{ij}$ are zero. The volume fraction α_i can be defined as follows.

- $\alpha_i = 0$: the cell is empty.
- $0 < \alpha_i < 1$: the interface is located in the cell.
- $\alpha_i = 1$: the cell is filled with phase i.

The sum of the volumetric fractions of each phase within the cells analyzed must be the unit.

$$\sum_{i=1}^{n}\alpha_i = 1 \quad (7)$$

From the previous concept, properties taken by a cell will be a mixture of the properties of the two phases weighted by the volume fraction of each of the phases. The density and viscosity of a cell where the interface is located are calculated as follows.

$$\rho = \alpha_i\rho_i + (1-\alpha_i)\rho_j \quad (8)$$

$$\mu = \alpha_i\mu_i + (1-\alpha_i)\mu_j \quad (9)$$

Where ρ y μ are the density and viscosity in the cells occupied by two phases, respectively.

To calculate the surface tension force ($\vec{F}$) the continuum surface force model (CSF) is used [82]. The surface tension force is calculated, as shown in the Equation (10).

$$\vec{F} = \sigma_{ij} \frac{\rho \kappa_i \nabla \alpha_i}{\frac{1}{2}(\rho_i + \rho_j)} \tag{10}$$

where σ_{ij} is the coefficient of surface tension and κ_i is the curvature of the interface taken from inside the phase i. κ_i is defined in terms of the divergence of the unit vector of the phase i fraction gradient. The equations are as follows.

$$n = \nabla \alpha_i \tag{11}$$

$$\kappa_i = \nabla \cdot \hat{n} \tag{12}$$

where n is the normal vector to the interface surface and $\hat{n}$ is the unit vector. The phase wettability is used employing the contact angle to adjust the interface curvature in areas close to the walls of the micromodel.

$$\hat{n} = \hat{n}_w \cos\theta_i + \hat{t}_w \sin\theta_i \tag{13}$$

where $\hat{n}_w$ and $\hat{t}_w$ are the unit vectors normal and tangential to the wall of the micromodel and θ_i is the contact angle of phase i with the wall of the micro model.

For pressure-velocity coupling, the Pressure Implicit with Splitting of Operators (PISO) was used. The converge criterion was set to 0.001 for all the parameters (continuity and velocities). The effect of each equation in iterations was set with the under-relaxation factors shown in Table 9. For the convective terms, the Second-Order Upwind Scheme was used.

Table 9. Under-relaxation factors.

Variable	Under-relaxation factor
Pressure	0.7
Density	1
Body forces	1
momentum	0.3

The boundary conditions applied to the simulations were velocity inlet and pressure outlet. Other edges in micromodels, such as grain and main domain were considered walls with total wettability to oil ($\theta_{oil} = 0$). In this study, gravitational forces are not considered. Also, micromodels were saturated with crude oil at the initial state. The inlet and outlet ports are ubicated ant the left and right of geometries shown in Figure 2, respectively. The boundary conditions applied to the system were velocity inlet and pressure Outlet, the other edges were considered to be wall with a complete oil wettability ($\theta_{oil} = 0$). Variable Time step was used in all simulations with a global Courant number of 2. The characteristics used for the variable time step is shown in the following table.

Table 10. Characteristics for the Variable Time Step used in the simulations.

Characteristic	Value
Minimum Time Step Size (s)	0.0001
Maximum Time Step Size (s)	10
Minimum Step change factor	0.8
Maximum Step change factor	1.2
Initial Time Step size (s)	0.1

4. Results

4.1 Validation of numerical results

Numerical results were compared with experimental data for validating the mathematical model. In this research, the oil recovery factor, the breakthrough time, the fractal dimension of the flow pattern and entrapment effect at the breakthrough time were compared with experimental data from [28] and these variables were also analyzed in different scenarios in order to evaluate the expected trend with the results of the numerical simulation. Also, Darcy's law was used to validate the pressure drop. In this way, we sought to validate all the results obtained related to the variables to be analyzed in this investigation.

For the recovery factor and breakthrough time, surfactant injection process was simulated in the oil-saturated micromodel (c) with an injection velocity of 10 ft/day, the interfacial tension between the fluid and crude oil was 0.03 mN/m; these conditions were the same as the experimental test. The properties used in the validation simulations are showed in Table 8. Figure 6 show the comparison of numerical results with experimental data. Also, the

Table 11 shows the point values for the oil recovery factor at the breakthrough time and the breakthrough time in terms of pore volume of injected fluid for the experimental data and numerical results.

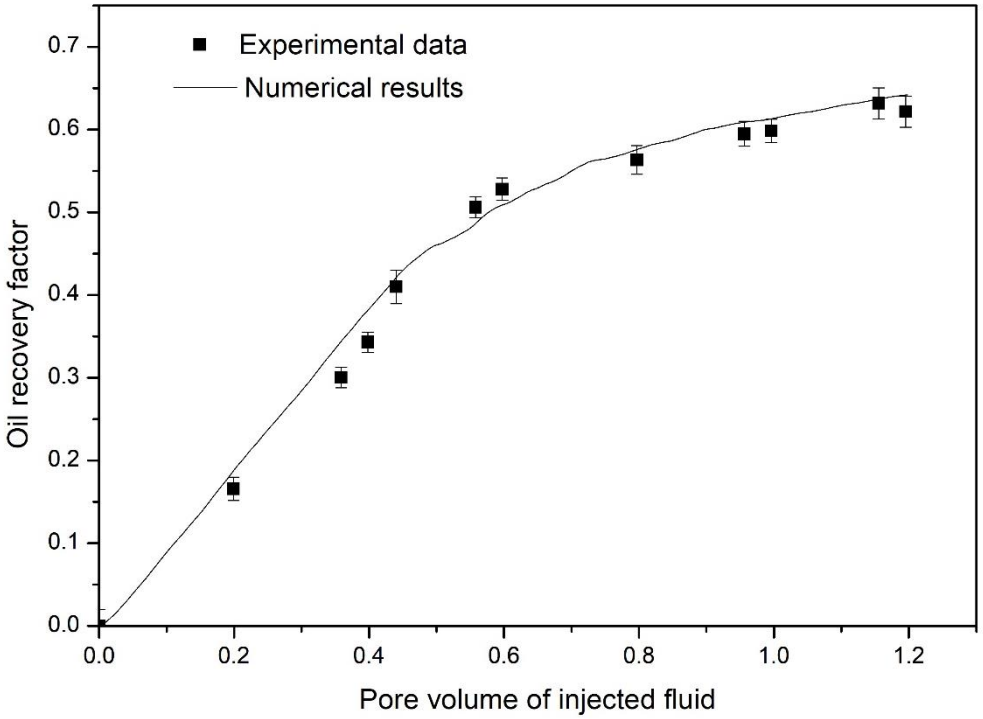

Figure 6. Comparison of numerical results with experimental data in the oil recovery factor.

Table 11. Comparison between experimental data and simulation results for the IFT case of 0.03 mN/m

System	Pore volume of injected fluid at the breakthrough time	Oil recovery factor at the breakthrough time
Experimental	0.50	0.47
Simulation	0.45	0.41

From the Table 11, it can be seen that the numerical results are in good agreement with the experimental data, the relative error in the oil recovery factors at the breakthrough time was 10% and the relative error in the breakthrough time was 12.7%. Although there are error rates greater than 10% in the points of interest where the recovery factor and the breakthrough time were evaluated, in Figure 6 it can be seen that the simulation has the

same trend or behavior as the experimental data, which it was something sought after by the numerical simulation of the process.

To complement the analysis carried out, the fractal dimension of the advancing front is also calculated for the simulation and experimental data. Figure 7 shows the distribution of fluids at rupture time.

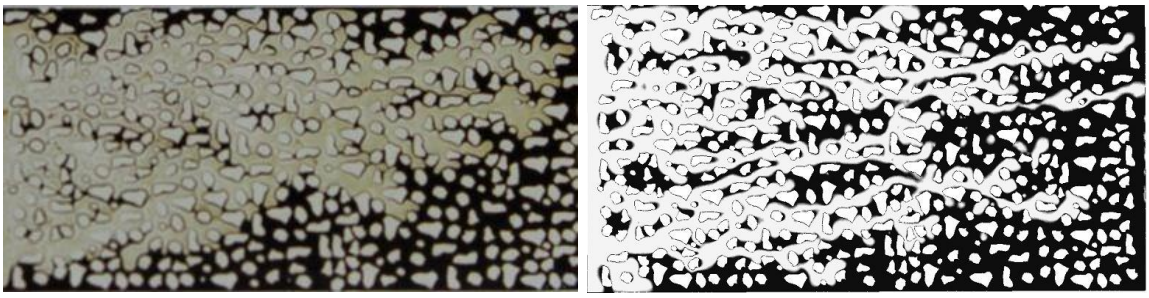

(a) (b)

Figure 7. Flow distribution within the micromodel at rupture time for testing with injection speed of 10 ft / day and IFT 0.03 mN / m. (a) Experimental (B) simulation.

The fractal dimension of flow pattern at the breakthrough time was calculated using image analysis. The fractal box counting method was applied to the images. the fractal dimension for the experimental test was 1.85, while this value for the numerical simulation was 1.83. the difference between these values lies in the way in which in the experimental test the fluid retains a front of advance with less interdigitation, while in the numerical simulation extensions of the fluid are presented, although the front in this case occupies more space within the micromodel.

For the validation of the model, numerical simulations were also performed at different IFT conditions. The recovery factor, breakthrough time, fractal dimension of the flow pattern and entrapment effect were compared in a surfactant injection process in the oil-saturated micromodel (c) with an injection velocity of 10 ft/day. the interfacial tension between the fluid and crude oil was 2.7 mN/m. Table 12 summarizes the results obtained for this case and Figure 8 shows the distribution of fluids.

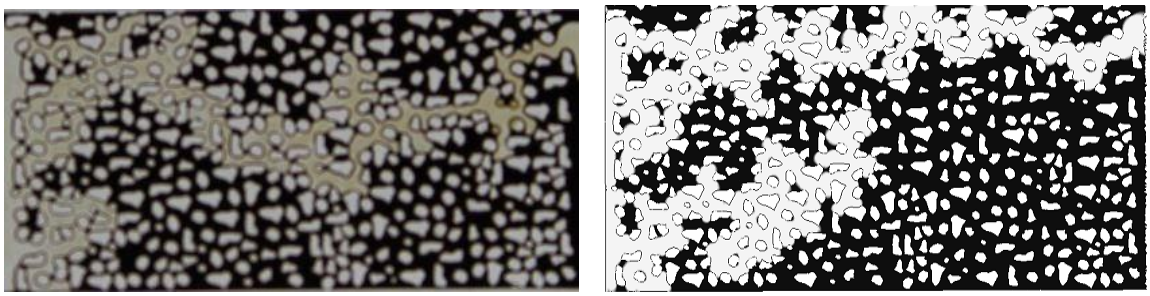

(a) (b)

Figure 8. Flow distribution within the micromodel at rupture time for testing with injection speed of 10 ft / day and IFT 2.7 mN / m. (a) Experimental (B) simulation.

Table 12. Comparison between experimental data and simulation results for the IFT case of 2.7 mN/m

System	Pore volume of injected fluid at the breakthrough time	Oil recovery factor at the breakthrough time	Fractal dimension of the flow pattern	Entrapment effect
Experimental	0.26	0.375	1.72	0.0397
Simulation	0.26	0.362	1.76	0.0417

For this case, there are no significant differences when comparing the breakthrough time of the experimental test with the numerical simulation. Considering the recovery factor, a relative error of 3.5% is obtained, which is a low value and is acceptable for model validation. The difference that occurs in the fractal dimension is explained by the form that the advance front takes in both cases, for the experimental test, the fluid occupies the central part of the micromodel, creating a preferential path and reducing its expansion within the device. On the other hand, in the numerical simulation, two advance fronts are formed, the first at the top of the device and the second by the central part. At breakthrough time, the path occupied by the upper part reaches the micromodel outlet, while the fluid that occupies the central part has a significant advance, which gives it a greater fractal dimension when compared with the experimental test. Considering the entrapment effect, there is a relative error of 5.03%. The effect of the interfacial tension of the surfactant with the crude oil and the wettability of the medium is well reflected in the numerical simulation.

For the pressure drop in the porous medium, because no experimental data were available, the process was validated based on Darcy's law, which considers the pressure drop in porous media based on velocity of displacement, the characteristics of the medium and the

viscosity of the fluid moving through the porous medium. Darcy's law is shown in the following equation.

$$\Delta P = \frac{\mu V}{K}\Delta x \tag{14}$$

where ΔP is the pressure drop across the porous medium, μ is the viscosity of the fluid moving through the porous medium, V is the velocity of the fluid, K is the absolute permeability of the porous medium, and Δx is the distance or length in the direction of movement of the fluid in the porous medium. Applying the Darcy's law to a case of water injection with a speed of 1 ft / day, with the permeability of the medium of 5.71 D and a distance of 2.65 cm, a pressure drop of 11.76 Pa is obtained. Performing the numerical simulation of this case through CFD, a total pressure drop of 11.96 Pa is obtained, this is shown in Figure 9. The pressure drop shown in figure 9 is obtained through the solution of the Navier-Stokes equation shown in equation (5), in this the pressure drop due to different factors such as viscosity and velocity is considered. On the other hand, it should be noted that Darcy's law does not consider other phenomena that cause a pressure drop, such as inertial effects or pressure drop due to the change in fluid velocity in the different directions of the micromodel, Darcy's law considers only an average velocity within the porous medium. Thus, when calculating the pressure drop from CFD simulations, different phenomena are considered that are not taken into account with the use of Darcy's law. Finally, when comparing the results obtained for both cases, a relative error of 1.7% is obtained, indicating the good capacity of the numerical model to replicate the results obtained experimentally.

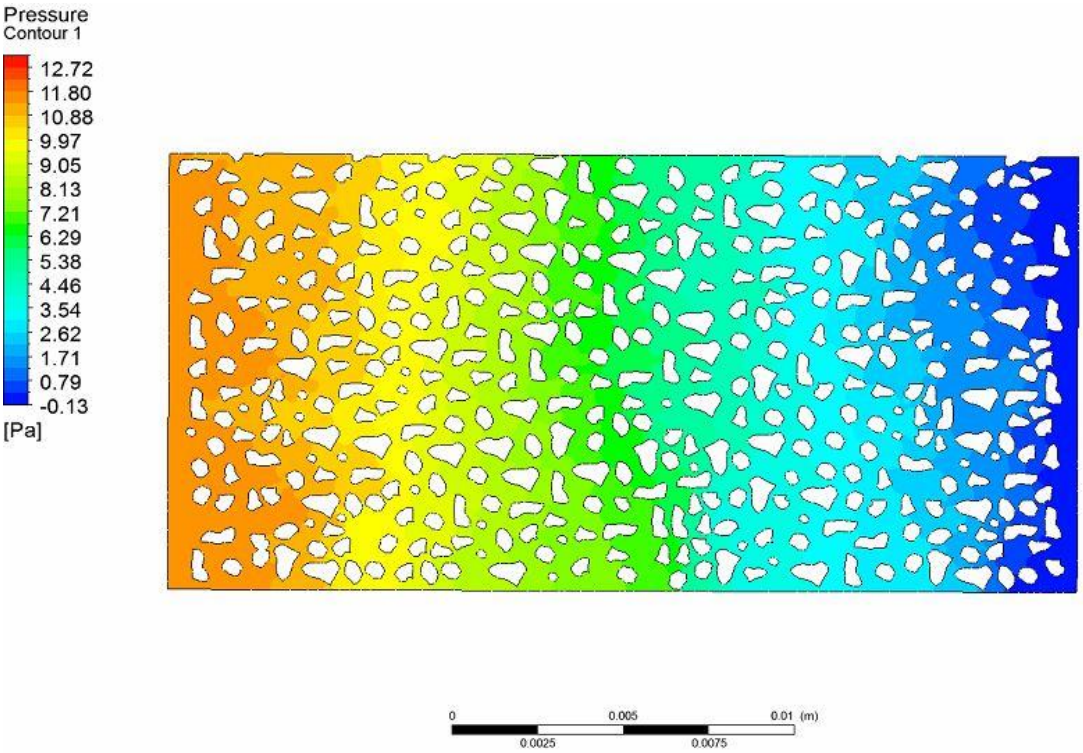

Figure 9. Pressure contour for water injection at 1 ft / day.

4.2 Micromodel selection flowchart for the evaluation of CEOR processes with surfactant injection

Based on the information collected in the literature on micromodels and the application of CFD simulations in injection processes with surfactants, the following selection flowchart for micromodels is propose.

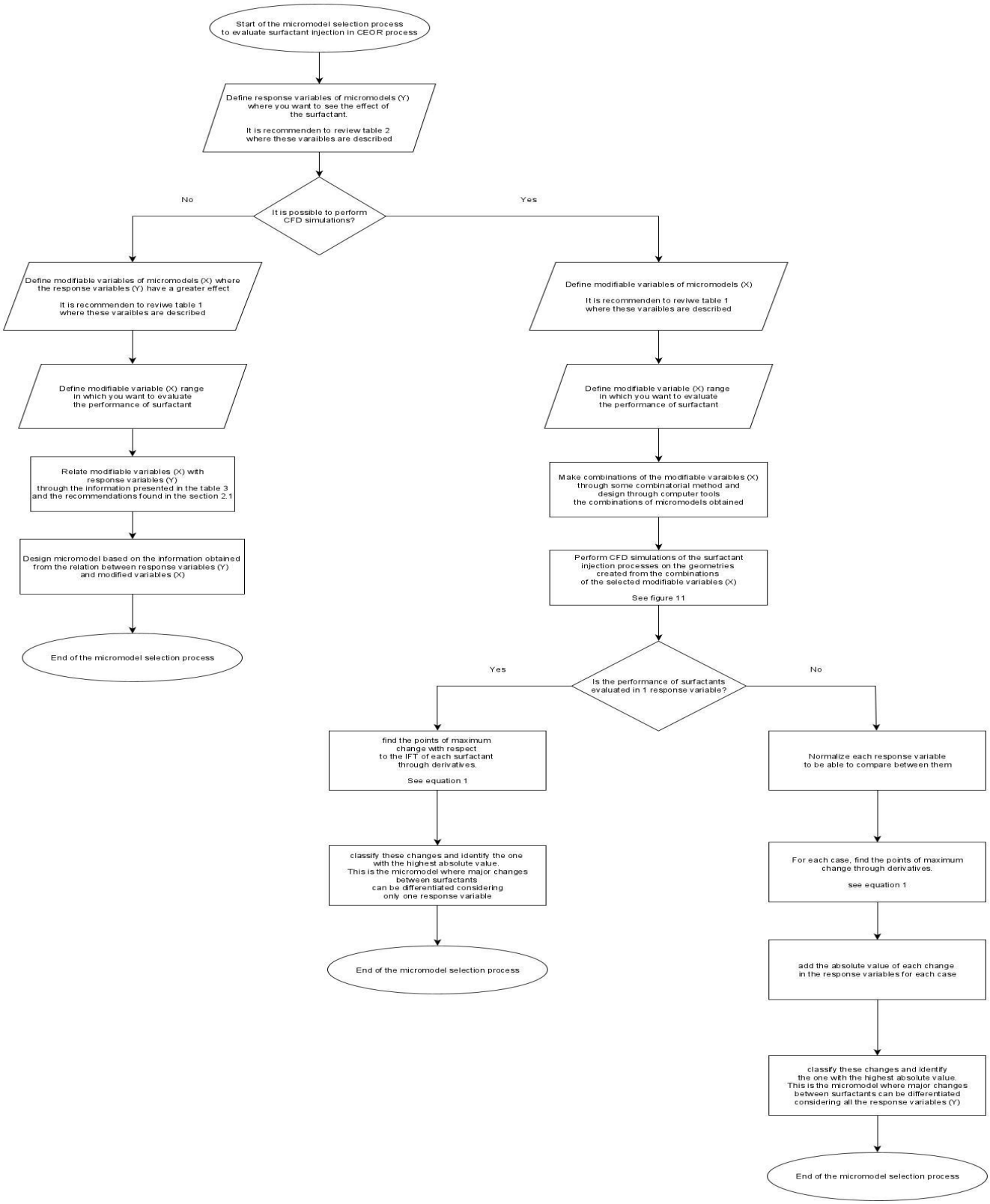

Figure 10. Selection flowcharts for micromodels for the evaluation of surfactant injection.

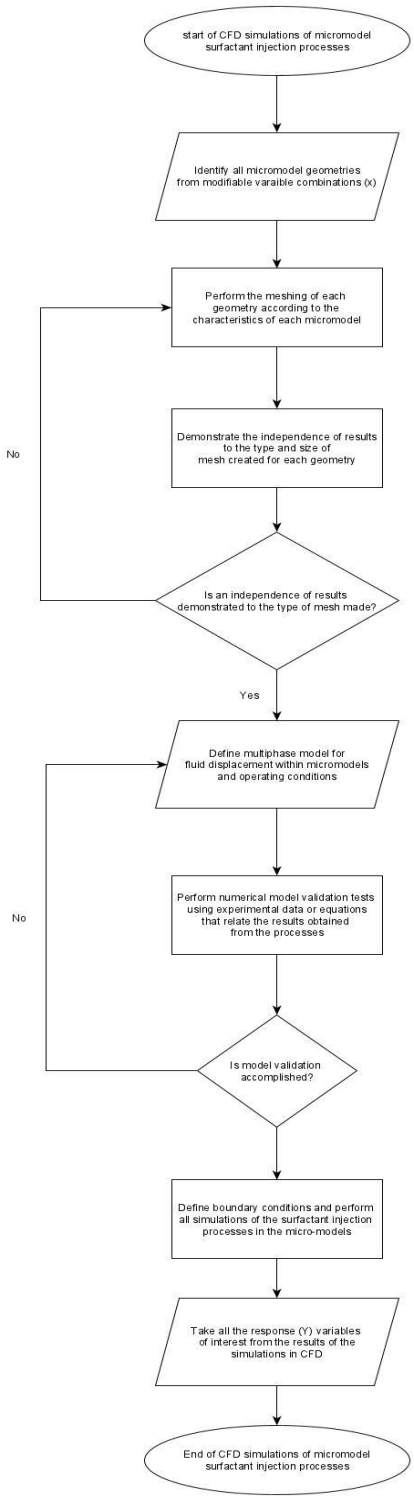

Figure 11. Flowchart for CFD simulation process.

Figure 11 explains the simulation application process through the CFD technique. This figure serves as a guide when the CFD application is available.

Figure 10 explains the selection flowchart of a micromodel based on the information obtained in literature or the availability of simulations in CFD. In the flowchart shown in Figure 10 the selection path can be highlighted when the application of CFD simulations is not available. For this case, the information shown in section 2.1, where the modifiable variables and response variables of a micro-model are related, is useful because it facilitates the process of selecting micromodels. The application of this flowchart is applied in the following section with the simulations carried out in this investigation, where four modifiable variables are involved in the micromodels (porosity, grain shape, presence of fracture and injection speed) on five response variables (Recovery factor, breakthrough time, fractal dimension, pressure drop and entrapment effect).

4.3 Micromodel selection flowchart application through CFD simulations

When the application of CFD simulations is available, it is possible to modify different variables in the micromodels, this due to the ease that design software present. A computer, as a drawing and process simulation tool, allows evaluating different characteristics that at an experimental level would have high consumption of resources and time.

32 cases evaluated for this investigation are shown in Table 4 with the results obtained from the simulations carried out through CFD. The description of each case and how these were obtained can be seen in section 3.1. From the factorial design of experiments, it was possible to identify 4 cases which are described below.

Case 1, non-fracture micromodels with circular grain shape and non-fracture; Case 2, non-fracture micromodels with irregular grain shape; Case 3, fractured micromodels with circular grain shape; and Case 4, fractured micromodels with irregular grain shape.

To quantify the effect of the surfactant for each evaluated case, the difference between the variable of interest (recovery factor, breakthrough time, fractal dimension, pressure drop,

entrapment effect) was evaluated and divided by the difference in interfacial tension between the surfactants evaluated (Equation 1). This was done in order to find points where the greatest change can be identified. In addition, to normalize the results, each difference was divided by the highest value obtained from each response variable shown in Table 4. In this way, Table 13 shows the cases treated for each micromodel and the absolute value of each normalized change obtained in the response variables of interest.

Table 13. Normalized results from CFD simulations.

Case	Grain shape	porosity	Injection velocity (ft/day)	Presence of fracture	Normalized recovery factor change	Nominalized breakthrough time change	Normalized fractal dimension change	Normalized Pressure drop change	Normalized entrapment effect change	Total
1	circular	0.5	10	no	0.5849	0.8042	0.7299	0.1211	5.1671	7.4072
	circular	0.7	10	no	1.4893	1.8510	0.1229	0.0006	0.4155	3.8794
	circular	0.5	30	no	3.0542	3.3109	0.8672	0.3691	1.5144	9.1158
	circular	0.7	30	no	14.2402	15.1789	1.9512	0.0051	11.0084	42.3838
2	irregular	0.5	10	no	3.1801	8.9666	0.3758	0.5139	7.7157	20.7520
	irregular	0.7	10	no	2.2359	1.7450	0.5275	0.0675	23.9375	28.5134
	irregular	0.5	30	no	5.4383	3.4271	0.4047	1.8207	35.7587	46.8495
	irregular	0.7	30	no	5.4767	6.1025	0.3324	1.6719	4.8316	18.4151
3	circular	0.5	10	yes	2.4007	2.1866	0.1518	0.1518	7.6710	12.5618
	circular	0.7	10	yes	1.4997	1.5699	0.9322	0.0821	0.4426	4.5265
	circular	0.5	30	yes	2.7629	1.2247	0.0217	0.0868	75.5805	79.6766
	circular	0.7	30	yes	1.3589	1.6231	0.5998	0.0310	3.2303	6.8431
4	irregular	0.5	10	yes	2.4098	3.0566	1.0190	1.9737	13.0414	21.5005
	irregular	0.7	10	yes	1.0688	1.1607	2.6305	0.2622	2.7455	7.8678
	irregular	0.5	30	yes	1.9258	1.6677	1.3442	3.0821	18.7241	26.7438
	irregular	0.7	30	yes	1.7913	2.7149	0.6070	1.2656	7.1165	13.4953

From the results shown in Table 13, it is possible to identify the points where there are greater changes in the variables of interest with surfactants in the range of IFT evaluated.

Table 14 shows a summary for each response variable and for each case, where it is in greatest change within the range of variables evaluated.

Table 14. Conditions of greater and minor change in the performance of surfactants in cases evaluated

Case	Recovery factor		breakthrough time		Fractal dimension		Pressure drop change		Entrapment Effect	
	Biggest change	**minor change**	**Biggest change**	**minor change**	**Biggest change**	**minor change**	**Biggest change**	**minor change**	**Biggest change**	**minor change**
Circular grain shape and non-fracture micromodel	High velocity injection - High porosity	Low velocity injection - Low porosity	High velocity injection - High porosity	Low velocity injection - Low porosity	High velocity injection - High porosity	Low velocity injection - high porosity	High velocity injection - low porosity	High velocity injection - High porosity	High velocity injection -high porosity	low velocity injection - high porosity
Irregular grain shape and non-fracture micromodel	High velocity injection	Low velocity injection	Low velocity injection - Low porosity	Low velocity injection - High porosity	Low velocity injection - high porosity	High velocity injection - High porosity	High velocity injection - low porosity	low velocity injection - high porosity	High velocity injection - low porosity	High velocity injection -high porosity
circular grain shape and fractured micromodel	Low velocity injection - Low porosity	High velocity injection - High porosity	Low velocity injection - Low porosity	high velocity injection - Low porosity	Low velocity injection - High porosity	high velocity injection - low porosity	low velocity injection - low porosity	high velocity injection - high porosity	High velocity injection - low porosity	low velocity injection - high porosity
irregular grain shape and fractured micromodel	Low velocity injection - Low porosity	Low velocity injection - high porosity	Low velocity injection - Low porosity	Low velocity injection - high porosity	Low velocity injection - High porosity	High velocity injection - High porosity	high velocity injection - low porosity	low velocity injection - high porosity	High velocity injection - low porosity	low velocity injection - high porosity

In this way, with the information presented in Table 14, it is possible to choose scenarios and conditions in micromodels where their performance is evaluated and differentiated. Table 15 shows the results obtained when all the changes in the response variables (Y) are considered. This means, when the performance of the surfactants is evaluated considering all the response variables (Y).

Table 15. Summary of results for the cases evaluated

Case	Changes considering the effect of all response variables (Y)	
	Biggest change	**minor change**
Circular grain shape and non-fracture micromodel	High velocity injection - High porosity	low velocity injection - High porosity
Irregular grain shape and non-fracture micromodel	High velocity injection - low porosity	High velocity injection - High porosity
circular grain shape and fractured micromodel	High velocity injection - low porosity	low velocity injection - High porosity
irregular grain shape and fractured micromodel	High velocity injection - low porosity	low velocity injection - High porosity

Considering the results shown in Table 15, for the cases treated in this investigation, different conditions are proposed to achieve the greatest difference between the performance of each surfactant, in this way, it is possible to obtain a microfluidic device where it can be evaluated the performance of surfactants in an ultra-low range, where their properties are similar considering different responses of the injection process.

Finally, from the information shown in the table, it is possible to choose a micromodel among the 8 evaluated in this research, where the greatest difference is found considering all the response variables. In this way, the micromodel where a greater difference is shown for this case, is the micromodel with a low porosity (0.5), a high injection velocity (30ft/day), with a circular grain shape (circular) and with presence fracture. This is the micromodel e, which can be seen in Figure 2.

In this way, the choice of a micromodel is achieved based on a methodology presented from a flowchart. The application of CFD allows evaluating a greater number of modifiable variables due to the ease presented by design software. On the other hand, regarding the application of CFD, the meshing procedure and validation of results must be taken into

account, where changes in modifiable variables such as porosity, presence of fracture or grain shape can change the type of mesh to be used, which would consume more computing time

5. Conclusions

In this research, the enhanced oil recovery was simulated with surfactant injection into multiples micromodels that have different geometry properties using the CFD technique. The geometries were created using Matlab and CorelDraw software. The governing equations, along with the VOF multiphase model, were solved using Ansys Fluent 19.1 software. The mathematical model was validated by experimental data. The factorial experimental design (2^5) was used to combine the chosen modifiable variables of micromodels for evaluating the effect of different characteristics on the response variables. In addition, a micromodel selection flowchart was designed and implemented to evaluate the performance of surfactants with simulated properties in the ultra-low interfacial tension range. Also, this selection flowchart could be used when the application of CFD is not available through the information found within this research. From the development of this investigation, the following conclusions are described:

- The combination between numerical simulation techniques such as CFD with new technologies such as microfluidics, allows a better understanding of CEOR processes with surfactant injection.
- The application of a selection flowchart of micromodels facilitates the work for the design and the experimental tests, allowing a possible saving of resources and time.
- From a compilation of research carried out on the use of micromodels for the evaluation of crude oil displacement processes, it was possible to identify a relation between modifiable variables and response variables of a micromodel. This relation can be seen in Table 3
- Within the range of the modifiable variables of a micromodels (X), the development of this investigation allowed to identify a micromodel, with geometric and operational characteristics, which allows to identify differences between the performance of surfactants with similar properties.

Acknowledgment

The authors acknowledge COLCIENCIAS, ANH, and Universidad Nacional de Colombia for their financing and logistic support provided by agreement 064-2018.

6. Appendix

Meshing of the geometries considered for this investigation

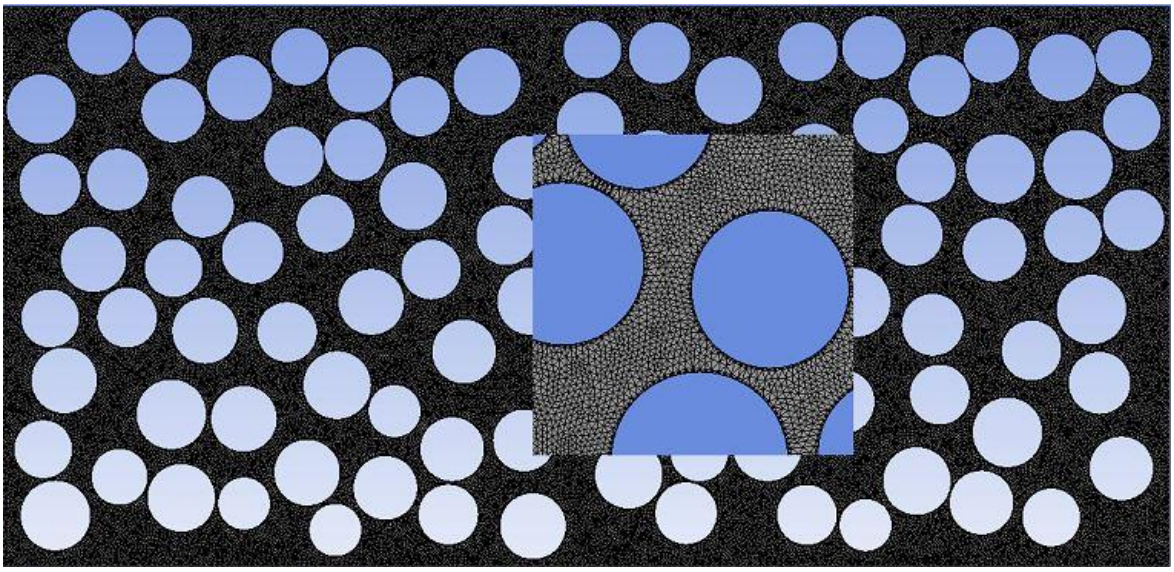

Figure 12. Meshing of the micromodel A geometry.

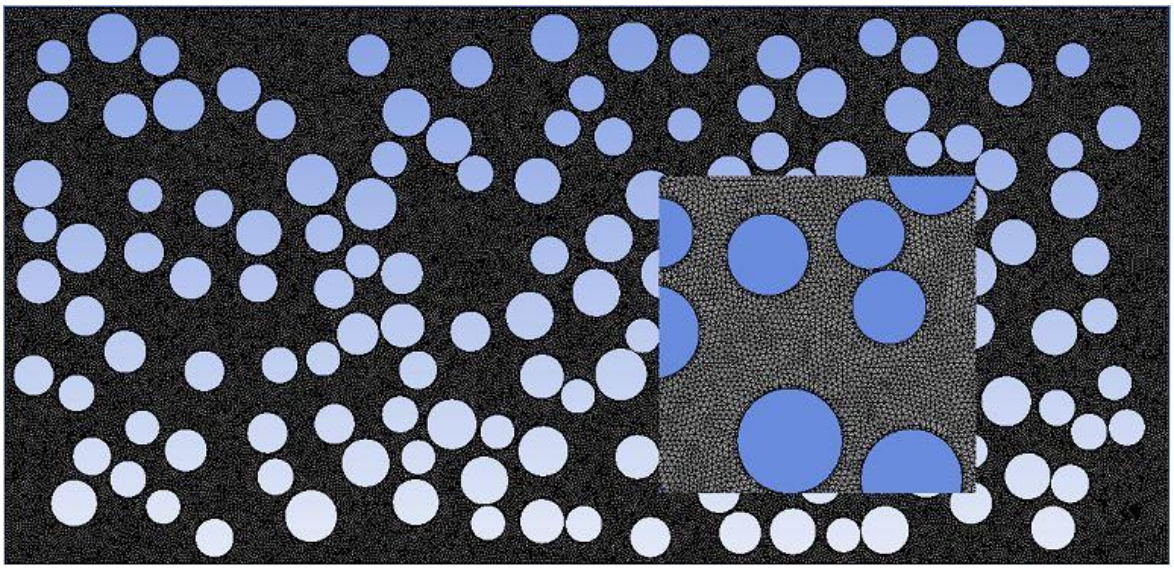

Figure 13. Meshing of the micromodel B geometry.

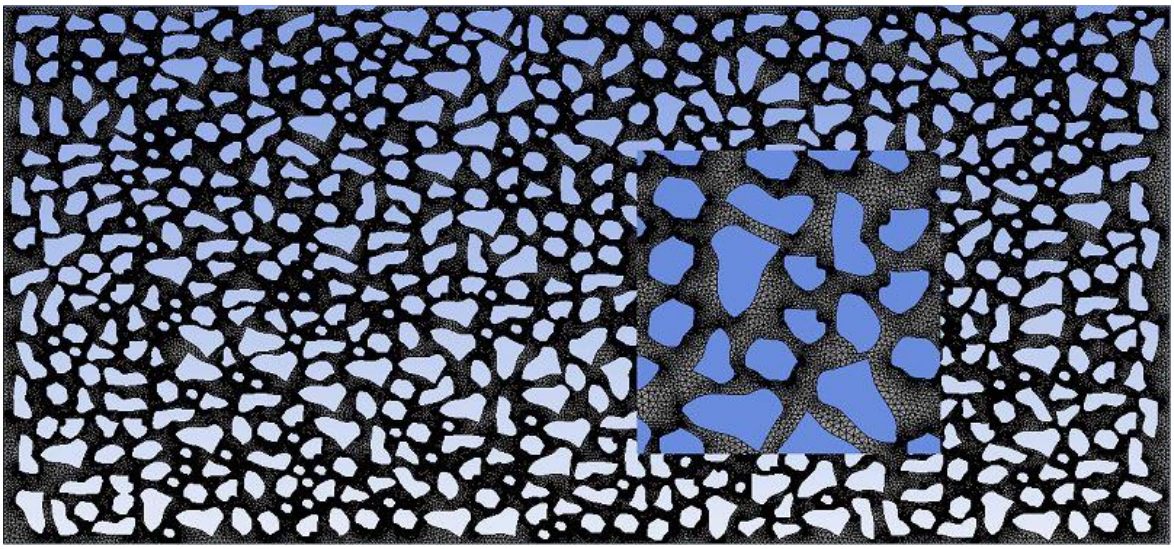

Figure 14. Meshing of the micromodel C geometry.

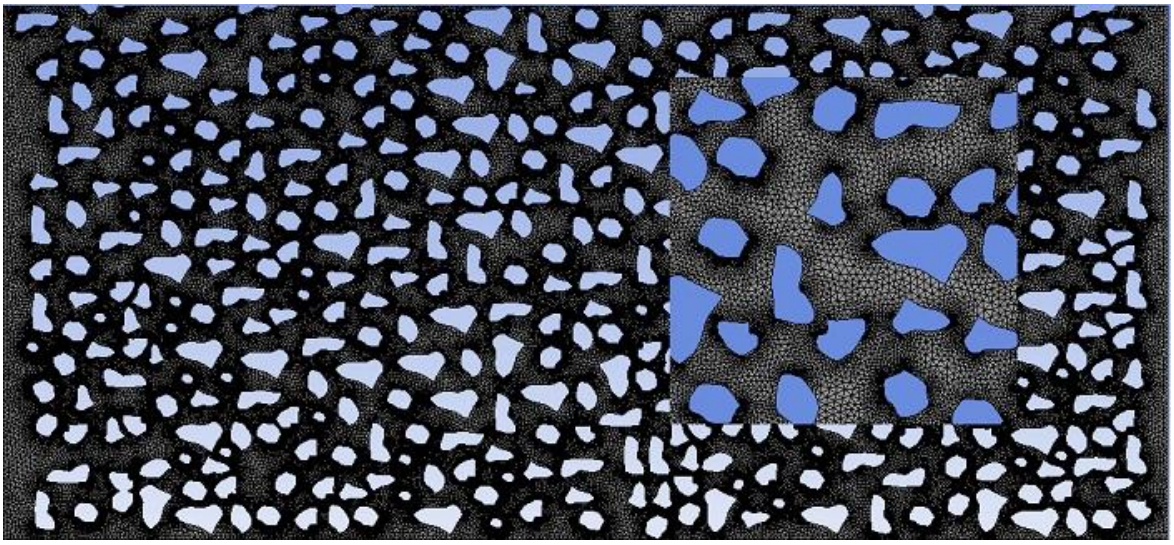

Figure 15. Meshing of the micromodel D geometry.

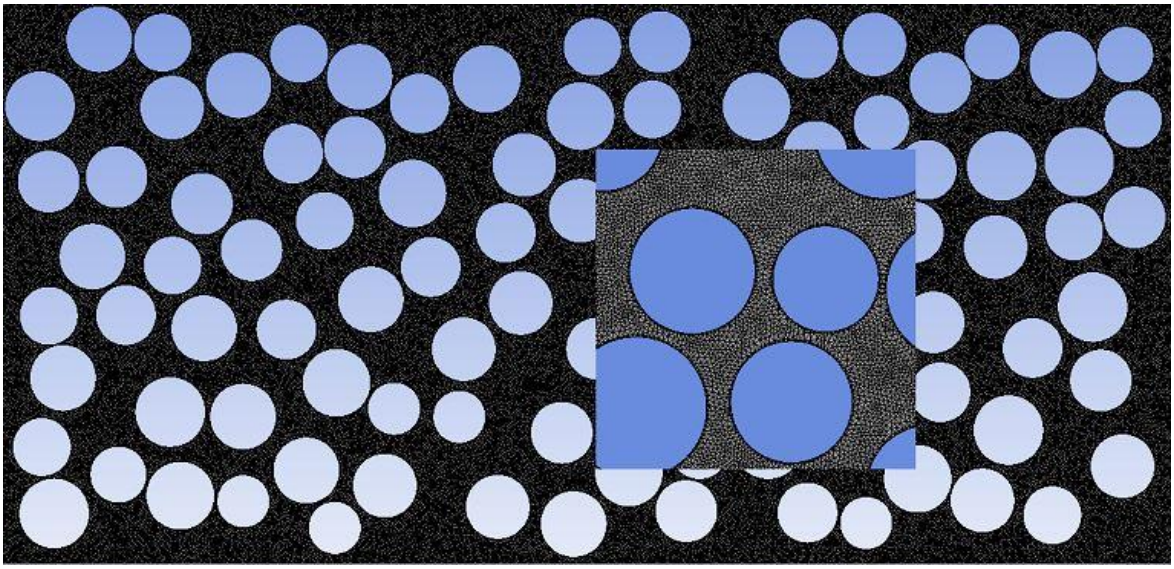

Figure 16. Meshing of the micromodel E geometry.

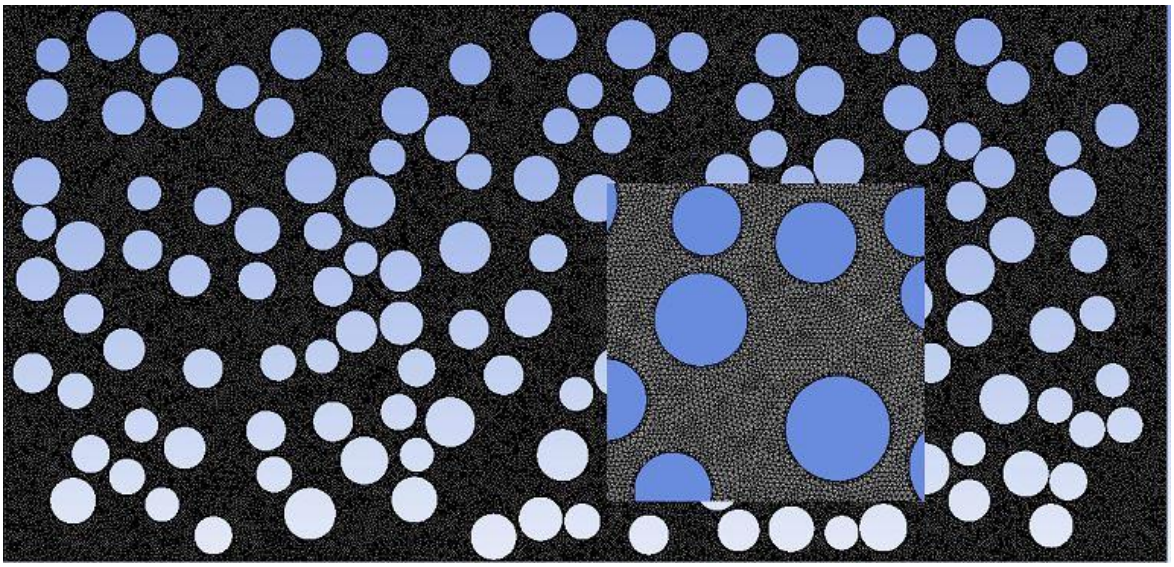

Figure 17. Meshing of the micromodel F geometry.

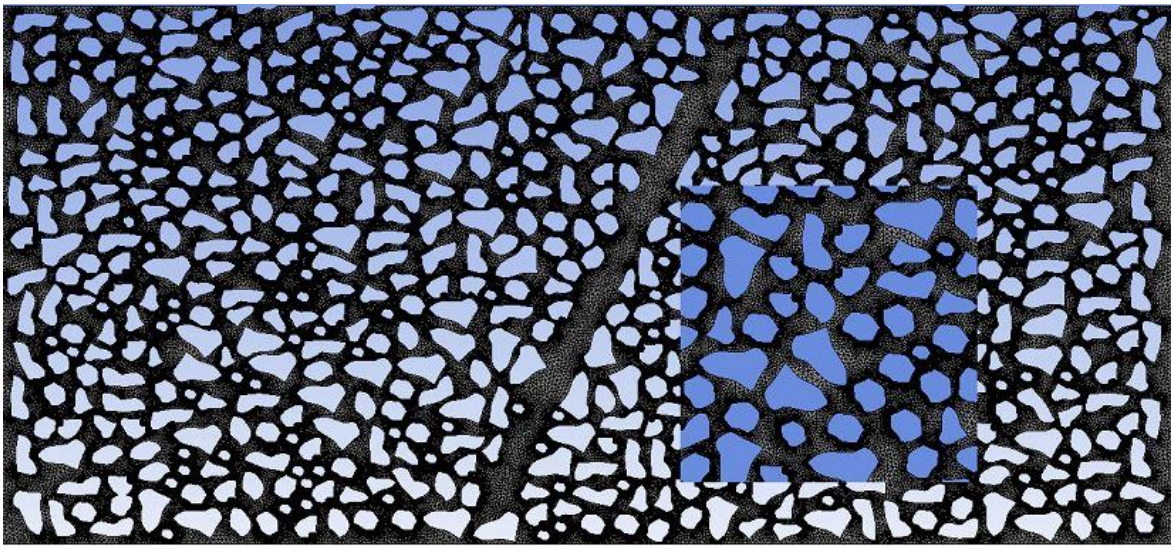

Figure 18. Meshing of the micromodel G geometry.

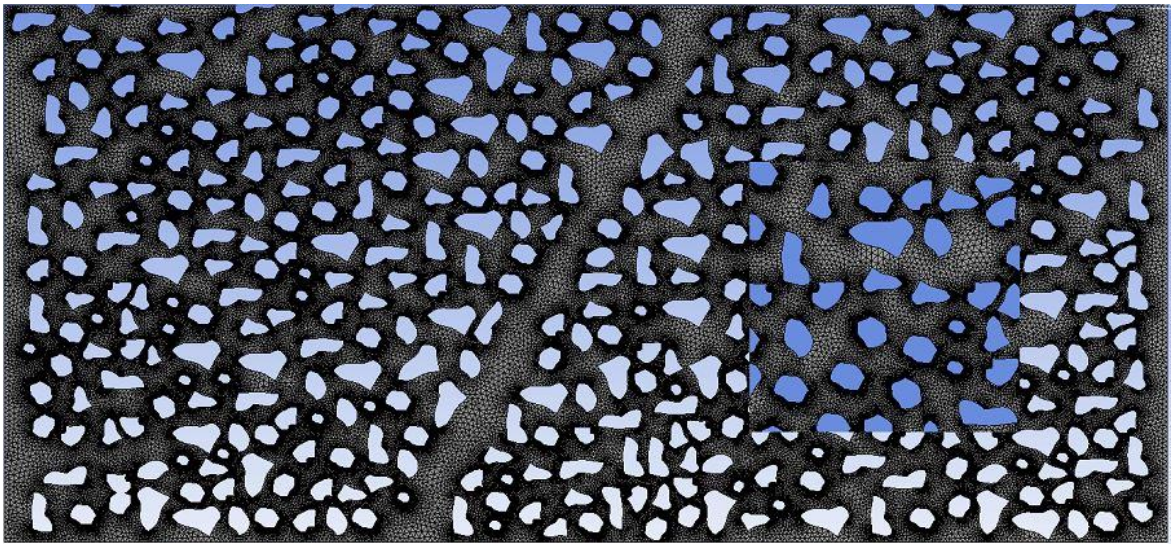

Figure 19. Meshing of the micromodel H geometry.

3. Conclusions and recommendations

3.5 Conclusions

In this research, different characteristics that affect the CEOR processes with surfactant injection in microfluidic devices were investigated through computational fluid dynamics simulation in order to apply a selection flowchart and obtain a micromodel that allows evaluating the performance of surfactant within the chosen ranges of the variables selected in this research. The conclusions of this research are as follow:

- The use of computational fluid dynamics helps to improve the processes carried out experimentally, allowing us to analyze different geometries and configurations in micromodels.
- Analysis of the modification of characteristics was obtained from the combination between the computational fluid dynamics and the factorial experimental design. This was used to understand better the processes performed on micromodels.
- The application of a selection flowchart of micromodels facilitates the work for the design and the experimental tests, allowing a possible saving of resources and time.
- From a compilation of research carried out on the use of micromodels for the evaluation of crude oil displacement processes, it was possible to identify a relation between modifiable variables and response variables of a micromodel. This relation can be seen in Table 3 in Chapter 2.
- Within the range of the modifiable variables of a micromodels (X), the development of this investigation allowed to identify a micromodel, with geometric and operational characteristics, which allows to identify differences between the performance of surfactants with similar properties.

3.6 Recommendations

From the results obtained in this research, the following recommendations are made:

- Expand the range of modifiable variables. For instance, a lower porosity or other type of grain shape (triangular or square).
- Include other modifiable variables of importance in micromodels that represent petrophysical properties in the analysis, for instance, the wettability of the material.
- Include changing displacing fluid properties in the analysis to extend the application of selection flowchart, for instance, density or viscosity.
- Analyze the performance of surfactant with this methodology when modifying the properties of crude oil.
- Evaluate different initial saturation states in the micromodels.

References

[1] J. M. Harris and B. Roach, *Environmental and natural resource economics: A contemporary approach*. Routledge, 2017.

[2] S. Thomas, "Enhanced oil recovery-an overview," *Oil & Gas Science and Technology-Revue de l'IFP,* vol. 63, no. 1, pp. 9-19, 2008.

[3] J. J. Sheng, "Status of surfactant EOR technology," *Petroleum,* vol. 1, no. 2, pp. 97-105, 2015.

[4] D. Levitt *et al.*, "Identification and evaluation of high-performance EOR surfactants," in *SPE/DOE Symposium on Improved Oil Recovery*, 2006: Society of Petroleum Engineers.

[5] C. A. Conn, "The characterization and visualization of multi-phase systems using microfluidic devices," 2015.

[6] A. Howe, A. Clarke, J. Mitchell, J. Staniland, and L. Hawkes, "Visualising surfactant EOR in core plugs and micromodels," in *SPE Asia Pacific enhanced oil recovery conference*, 2015: Society of Petroleum Engineers.

[7] A. M. Howe, A. Clarke, J. Mitchell, J. Staniland, L. Hawkes, and C. Whalan, "Visualising surfactant enhanced oil recovery," *Colloids and Surfaces A: Physicochemical and Engineering Aspects,* vol. 480, pp. 449-461, 2015.

[8] S. Gogoi and S. B. Gogoi, "Review on microfluidic studies for EOR application," *Journal of Petroleum Exploration and Production Technology,* pp. 1-15, 2019.

[9] N. Karadimitriou and S. Hassanizadeh, "A review of micromodels and their use in two-phase flow studies," *Vadose Zone Journal,* vol. 11, no. 3, 2012.

[10] V. A. Lifton, "Microfluidics: an enabling screening technology for enhanced oil recovery (EOR)," *Lab on a Chip,* vol. 16, no. 10, pp. 1777-1796, 2016.

[11] E. M. Chapman, "Microfluidic visualisation and analysis of multiphase flow phenomena at the pore scale," 2014.

[12] E. D. Vavra, Y. Zeng, S. Xiao, G. J. Hirasaki, and S. L. Biswal, "Microfluidic Devices for Characterizing Pore-scale Event Processes in Porous Media for Oil Recovery Applications," *JoVE (Journal of Visualized Experiments),* no. 131, p. e56592, 2018.

[13] J. Wan, T. K. Tokunaga, C. F. Tsang, and G. S. Bodvarsson, "Improved glass micromodel methods for studies of flow and transport in fractured porous media," *Water resources research,* vol. 32, no. 7, pp. 1955-1964, 1996.

[14] P. Lele, H. Fadaei, U. Guerrero, and D. Sinton, "Development of a microfluidic device for rapid assessment of EOR additives," in *SPE Heavy Oil Conference-Canada*, 2014: Society of Petroleum Engineers.

[15] G. Rosero *et al.*, "Design and analysis of different models of microfluidic devices evaluated in Enhanced Oil Recovery (EOR) assays," *Matéria (Rio de Janeiro),* vol. 23, no. 2, 2018.
[16] M. Mahmoodi, "Micromodel method for enhanced oil recovery; fabrication and image processing," Memorial University of Newfoundland, 2017.
[17] A. Gerami *et al.*, "Microfluidics for porous systems: fabrication, microscopy and applications," *Transport in Porous Media,* pp. 1-28, 2018.
[18] A. Anbari, H. T. Chien, S. S. Datta, W. Deng, D. A. Weitz, and J. Fan, "Microfluidic model porous media: fabrication and applications," *Small,* vol. 14, no. 18, p. 1703575, 2018.
[19] D. S. Park, S. Bou-Mikael, S. King, K. E. Thompson, C. S. Willson, and D. E. Nikitopoulos, "Design and fabrication of rock-based micromodel," in *ASME 2012 International Mechanical Engineering Congress and Exposition*, 2012, pp. 709-715: American Society of Mechanical Engineers.
[20] W. Wang, S. Chang, and A. Gizzatov, "Toward reservoir-on-a-chip: fabricating reservoir micromodels by in situ growing calcium carbonate nanocrystals in microfluidic channels," *ACS applied materials & interfaces,* vol. 9, no. 34, pp. 29380-29386, 2017.
[21] A. Ferrari, J. Jimenez-Martinez, T. L. Borgne, Y. Méheust, and I. Lunati, "Challenges in modeling unstable two-phase flow experiments in porous micromodels," *Water Resources Research,* vol. 51, no. 3, pp. 1381-1400, 2015.
[22] T. Clemens, K. Tsikouris, M. Buchgraber, L. M. Castanier, and A. Kovscek, "Pore-Scale Evaluation of Polymers Displacing Viscous Oil--Computational-Fluid-Dynamics Simulation of Micromodel Experiments," *Spe Reservoir Evaluation & Engineering,* vol. 16, no. 02, pp. 144-154, 2013.
[23] S. Maaref, M. R. Rokhforouz, and S. Ayatollahi, "Numerical investigation of two phase flow in micromodel porous media: Effects of wettability, heterogeneity, and viscosity," *The Canadian Journal of Chemical Engineering,* vol. 95, no. 6, pp. 1213-1223, 2017.
[24] J. Wegner and L. Ganzer, "Rock-on-a-Chip Devices for High p, T Conditions and Wettability Control for the Screening of EOR Chemicals," in *SPE Europec featured at 79th EAGE Conference and Exhibition*, 2017: Society of Petroleum Engineers.
[25] K. Xu *et al.*, "A 2.5-D glass micromodel for investigation of multi-phase flow in porous media," *Lab on a Chip,* vol. 17, no. 4, pp. 640-646, 2017.
[26] H. K. Versteeg and W. Malalasekera, *An introduction to computational fluid dynamics: the finite volume method*. Pearson education, 2007.
[27] R. Gharibshahi, A. Jafari, A. Haghtalab, and M. S. Karambeigi, "Application of CFD to evaluate the pore morphology effect on nanofluid flooding for enhanced oil recovery," *RSC Advances,* vol. 5, no. 37, pp. 28938-28949, 2015.
[28] S. Betancur *et al.*, "A microfluidic study to investigate the effect of magnetic iron core-carbon shell nanoparticles on displacement mechanisms of crude oil for chemical enhanced oil recovery," p. 106589, 2019.

[29] F. J. N.-H. Escobar, Universidad Surcolombiana, "Aspectos fundamentales de recobro secundario y terciario," 2006.
[30] E. J. Manrique *et al.*, "EOR: current status and opportunities," in *SPE improved oil recovery symposium*, 2010: Society of Petroleum Engineers.
[31] J. Sheng, *Modern chemical enhanced oil recovery: theory and practice*. Gulf Professional Publishing, 2010.
[32] M. Sedaghat, O. Mohammadzadeh, S. Kord, and I. Chatzis, "Heavy oil recovery using ASP flooding: A pore-level experimental study in fractured five-spot micromodels," *The Canadian Journal of Chemical Engineering,* vol. 94, no. 4, pp. 779-791, 2016.
[33] D. Wever, F. Picchioni, and A. Broekhuis, "Polymers for enhanced oil recovery: a paradigm for structure–property relationship in aqueous solution," *Progress in Polymer Science,* vol. 36, no. 11, pp. 1558-1628, 2011.
[34] J. J. Sheng, "A comprehensive review of alkaline–surfactant–polymer (ASP) flooding," *Asia-Pacific Journal of Chemical Engineering,* vol. 9, no. 4, pp. 471-489, 2014.
[35] M. Mohajeri, M. Hemmati, and A. S. Shekarabi, "An experimental study on using a nanosurfactant in an EOR process of heavy oil in a fractured micromodel," *Journal of petroleum Science and engineering,* vol. 126, pp. 162-173, 2015.
[36] M. Dong, Q. Liu, and A. Li, "Displacement mechanisms of enhanced heavy oil recovery by alkaline flooding in a micromodel," *Particuology,* vol. 10, no. 3, pp. 298-305, 2012.
[37] H. Yarveicy and A. J. P. Javaheri, "Application of Lauryl Betaine in enhanced oil recovery: A comparative study in micromodel," vol. 5, no. 2, pp. 123-127, 2019.
[38] H. Hematpour, R. Arabjamloei, M. Nematzadeh, H. Esmaili, and M. Mardi, "An experimental investigation of surfactant flooding efficiency in low viscosity oil using a glass micromodel," *Energy Sources, Part A: Recovery, Utilization, and Environmental Effects,* vol. 34, no. 19, pp. 1745-1758, 2012.
[39] A. Chatenever and J. C. J. J. o. P. T. Calhoun Jr, "Visual examinations of fluid behavior in porous media-part i," vol. 4, no. 06, pp. 149-156, 1952.
[40] A. Rufai, "Porous media drying and two-phase flow studies using micromodels," 2018.
[41] Y. M. Corapcioglu, S. Chowdhury, and S. E. J. W. r. r. Roosevelt, "Micromodel visualization and quantification of solute transport in porous media," vol. 33, no. 11, pp. 2547-2558, 1997.
[42] C. Tsakiroglou and D. J. J. o. m. s. Avraam, "Fabrication of a new class of porous media models for visualization studies of multiphase flow processes," vol. 37, no. 2, pp. 353-363, 2002.
[43] B. B. J. P. s. Mandelbrot, "Self-affine fractals and fractal dimension," vol. 32, no. 4, p. 257, 1985.

[44] J. T. Cheng, L. J. Pyrak-Nolte, D. D. Nolte, and N. J. J. G. R. L. Giordano, "Linking pressure and saturation through interfacial areas in porous media," vol. 31, no. 8, 2004.
[45] N. Mosavat and F. J. F. Torabi, "Micro-optical analysis of carbonated water injection in irregular and heterogeneous pore geometry," vol. 175, pp. 191-201, 2016.
[46] M. Borji, "Alkali-based Displacement Processes in Microfluidic Experiments: Application to the Matzen Oil Field."
[47] D. Park, S. Bou-Mikael, S. King, K. Thompson, C. Willson, and D. Nikitopoulos, "Design and Fabrication of Rock-Based Polymer Micromodel," in *Proc. ASME 2012 International Mechanical Engineering Congress & Exposition, ASME, Houston, TX, USA*, 2012, pp. 709-716.
[48] B. Sandnes, H. Knudsen, K. Måløy, and E. J. P. r. l. Flekkøy, "Labyrinth patterns in confined granular-fluid systems," vol. 99, no. 3, p. 038001, 2007.
[49] G. Løvoll *et al.*, "Influence of viscous fingering on dynamic saturation–pressure curves in porous media," vol. 86, no. 1, pp. 305-324, 2011.
[50] M. Wegner, J. J. P. Christie, and C. o. Minerals, "Chemical etching of deformation sub-structures in quartz," vol. 9, no. 2, pp. 67-78, 1983.
[51] K. Kolari, V. Saarela, S. J. J. o. M. Franssila, and Microengineering, "Deep plasma etching of glass for fluidic devices with different mask materials," vol. 18, no. 6, p. 064010, 2008.
[52] F. P. Melchels, J. Feijen, and D. W. J. B. Grijpma, "A review on stereolithography and its applications in biomedical engineering," vol. 31, no. 24, pp. 6121-6130, 2010.
[53] T. Hug, D. Parrat, P.-A. Kunzi, U. Staufer, E. Verpoorte, and N. F. de Rooij, "Fabrication of nanochannels with PDMS, silicon and glass walls and spontaneous filling by capillary forces," 2003.
[54] W. Soll, M. A. Celia, and J. J. W. r. r. Wilson, "Micromodel studies of three-fluid porous media systems: Pore-scale processes relating to capillary pressure-saturation relationships," vol. 29, no. 9, pp. 2963-2974, 1993.
[55] A. A. Keller, M. J. Blunt, and A. P. V. J. T. i. P. M. Roberts, "Micromodel observation of the role of oil layers in three-phase flow," vol. 26, no. 3, pp. 277-297, 1997.
[56] C. D. Montemagno and W. G. J. G. r. l. Gray, "Photoluminescent volumetric imaging: A technique for the exploration of multiphase flow and transport in porous media," vol. 22, no. 4, pp. 425-428, 1995.
[57] P. Rostami, M. Sharifi, B. Aminshahidy, and J. Fahimpour, "The effect of nanoparticles on wettability alteration for enhanced oil recovery: micromodel experimental studies and CFD simulation," *Petroleum Science,* pp. 1-15, 2019.
[58] S. Farzaneh, M. Ghazanfari, R. Kharrat, S. J. P. S. Vossoughi, and Technology, "An experimental and numerical investigation of solvent injection to heavy oil in fractured five-spot micromodels," vol. 28, no. 15, pp. 1567-1585, 2010.

[59] A. Danesh, D. Krinis, G. Henderson, J. J. J. o. P. S. Peden, and Engineering, "Pore-level visual investigation of miscible and immiscible displacements," vol. 2, no. 2-3, pp. 167-177, 1989.
[60] O. S. Owete and W. E. J. S. R. E. Brigham, "Flow behavior of foam: a porous micromodel study," vol. 2, no. 03, pp. 315-323, 1987.
[61] F. Mohammadi, A. Haghtalab, A. Jafari, and R. Gharibshahi, "CFD Study of Surfactant Flooding in a Micromodel with Quadratic Pore Shape," in *The 1st National Conference on Oil and Gas Fields Development (OGFD), 28-29 January, Tehran, Iran*, 2015.
[62] N. C. Wardlaw, "The effects of pore structure on displacement efficiency in reservoir rocks and in glass micromodels," in *SPE/DOE Enhanced Oil Recovery Symposium*, 1980: Society of Petroleum Engineers.
[63] T. W. Willingham, C. J. Werth, A. J. J. E. s. Valocchi, and technology, "Evaluation of the effects of porous media structure on mixing-controlled reactions using pore-scale modeling and micromodel experiments," vol. 42, no. 9, pp. 3185-3193, 2008.
[64] R. Gharibshahia, A. Jafaria, A. Haghtalaba, and M. S. Karambeigib, "Simulation of Nanofluid Flooding in a Micromodel with Quadratic Pore Shape Using CFD."
[65] A. Jafari, S. E. F. Pour, R. J. I. J. o. C. E. Gharibshahi, and Applications, "CFD Simulation of Biosurfactant Flooding into a Micromodel for Enhancing the Oil Recovery," vol. 7, no. 6, pp. 353-358, 2016.
[66] J. Zhao and D. J. R. a. Wen, "Pore-scale simulation of wettability and interfacial tension effects on flooding process for enhanced oil recovery," vol. 7, no. 66, pp. 41391-41398, 2017.
[67] J. Zhao, G. Yao, D. J. F. o. C. S. Wen, and Engineering, "Pore-scale simulation of water/oil displacement in a water-wet channel," pp. 1-12, 2019.
[68] B. Goudarzi, P. Mohammadmoradi, and A. Kantzas, "Pore-level simulation of heavy oil reservoirs; competition of capillary, viscous, and gravity forces," in *SPE Latin America and Caribbean Heavy and Extra Heavy Oil Conference*, 2016: Society of Petroleum Engineers.
[69] V. Bramer and W. Christopher, "Nanoparticle dispersion flow for enhanced oil recovery using micromodels," 2014.
[70] R. Gharibshahi, A. Jafari, H. J. J. o. P. S. Ahmadi, and Engineering, "CFD investigation of enhanced extra-heavy oil recovery using metallic nanoparticles/steam injection in a micromodel with random pore distribution," vol. 174, pp. 374-383, 2019.
[71] F. J. U. S. Escobar, "Fundamentos de ingeniería de yacimientos," 2000.
[72] M. A. Nilsson *et al.*, "Effect of fluid rheology on enhanced oil recovery in a microfluidic sandstone device," *Journal of Non-Newtonian Fluid Mechanics,* vol. 202, pp. 112-119, 2013.
[73] M. Karambeigi, M. Schaffie, M. J. P. s. Fazaelipoor, and technology, "Improvement of water flooding efficiency using mixed culture of

microorganisms in heterogeneous micro-models," vol. 31, no. 9, pp. 923-931, 2013.
[74] N. K. Karadimitriou, "Two-phase flow experimental studies in micro-models," UU Department of Earth Sciences, 2013.
[75] J. Cui and T. Babadagli, "Use of new generation chemicals and nano materials in heavy-oil recovery: Visual analysis through micro fluidics experiments," *Colloids and Surfaces A: Physicochemical and Engineering Aspects,* vol. 529, pp. 346-355, 2017.
[76] S. Ehrenberg, P. Nadeau, and Ø. J. A. b. Steen, "Petroleum reservoir porosity versus depth: Influence of geological age," vol. 93, no. 10, pp. 1281-1296, 2009.
[77] S. Ehrenberg and P. J. A. b. Nadeau, "Sandstone vs. carbonate petroleum reservoirs: A global perspective on porosity-depth and porosity-permeability relationships," vol. 89, no. 4, pp. 435-445, 2005.
[78] M. Buchgraber, M. Al-Dossary, C. Ross, A. R. J. J. o. P. S. Kovscek, and Engineering, "Creation of a dual-porosity micromodel for pore-level visualization of multiphase flow," vol. 86, pp. 27-38, 2012.
[79] M. Ghanad Dezfully, A. Jafari, and R. Gharibshahi, "CFD simulation of enhanced oil recovery using nanosilica/supercritical CO2," in *Advanced Materials Research*, 2015, vol. 1104, pp. 81-86: Trans Tech Publ.
[80] A. Minakov, E. Mikhienkova, M. Pryazhnikov, and V. Zhigarev, "Numerical simulation of the oil displacement process from a porous medium by nanofluid," in *Journal of Physics: Conference Series*, 2019, vol. 1382, no. 1, p. 012115: IOP Publishing.
[81] A. J. A. I. Fluent, USA, "Ansys fluent theory guide," vol. 15317, pp. 724-746, 2011.
[82] J. U. Brackbill, D. B. Kothe, and C. J. J. o. c. p. Zemach, "A continuum method for modeling surface tension," vol. 100, no. 2, pp. 335-354, 1992.
[83] J. J. J. P. Sheng, "Status of surfactant EOR technology," vol. 1, no. 2, pp. 97-105, 2015.
[84] C. T. Gerold, A. T. Krummel, and C. S. Henry, "Microfluidic devices containing thin rock sections for oil recovery studies," *Microfluidics and Nanofluidics,* vol. 22, no. 7, p. 76, 2018.
[85] M. Lv and S. J. R. A. Wang, "Pore-scale modeling of a water/oil two-phase flow in hot water flooding for enhanced oil recovery," vol. 5, no. 104, pp. 85373-85382, 2015.
[86] A. Timgren, G. Trägårdh, and C. J. C. e. s. Trägårdh, "Effects of cross-flow velocity, capillary pressure and oil viscosity on oil-in-water drop formation from a capillary," vol. 64, no. 6, pp. 1111-1118, 2009.
[87] M. Ferer, W. N. Sams, R. Geisbrecht, and D. H. J. A. J. Smith, "Fractal nature of viscous fingering in two-dimensional pore level models," vol. 41, no. 4, pp. 749-763, 1995.
[88] J. Nittmann, G. Daccord, and H. E. J. N. Stanley, "Fractal growth viscous fingers: quantitative characterization of a fluid instability phenomenon," vol. 314, no. 6007, pp. 141-144, 1985.

[89] A. Nabizadeh, M. Adibifard, H. Hassanzadeh, J. Fahimpour, and M. K. J. J. o. M. L. Moraveji, "Computational fluid dynamics to analyze the effects of initial wetting film and triple contact line on the efficiency of immiscible two-phase flow in a pore doublet model," vol. 273, pp. 248-258, 2019.

[90] K. XU, P. Zhu, C. Tatiana, C. Huh, and M. Balhoff, "A microfluidic investigation of the synergistic effect of nanoparticles and surfactants in macro-emulsion based EOR," in *SPE Improved Oil Recovery Conference*, 2016: Society of Petroleum Engineers.

[91] A. Afsharpoor, M. T. Balhoff, R. Bonnecaze, C. J. J. o. P. S. Huh, and Engineering, "CFD modeling of the effect of polymer elasticity on residual oil saturation at the pore-scale," vol. 94, pp. 79-88, 2012.

[92] H. Gutiérrez Pulido and R. d. l. Vara Salazar, "Análisis y diseño de experimentos," 2004.

[93] A. Ferrari, J. Jimenez-Martinez, T. L. Borgne, Y. Méheust, and I. J. W. R. R. Lunati, "Challenges in modeling unstable two-phase flow experiments in porous micromodels," vol. 51, no. 3, pp. 1381-1400, 2015.

[94] A. Q. Raeini, M. J. Blunt, and B. J. J. o. C. P. Bijeljic, "Modelling two-phase flow in porous media at the pore scale using the volume-of-fluid method," vol. 231, no. 17, pp. 5653-5668, 2012.